HELSINKI UNIVERSITY OF TECHNOLOGY
Department of Electrical and Communications Engineering
Laboratory of Computational Engineering

Teppo Häyrynen

Quantum Transport in the Ballistic and Coulomb Blockade Regimes

Master's thesis

Supervisor: Jukka Tulkki
Instructor Jukka Tulkki

Espoo 5th September 2003

Preface

The work for this master's thesis has been carried out at the Laboratory of Computational Engineering of the Helsinki University of Technology mainly during the winter, spring and summer of 2003. I want to thank professor Jukka Tulkki for his support and instruction during the whole work. I would also like to thank Kari Maijala for his advice.

Espoo, 5th September 2003

Teppo Häyrynen

Teppo Häyrynen

HELSINKI UNIVERSITY OF TECHNOLOGY

ABSTRACT OF THE MASTER'S THESIS

Author:	Teppo Häyrynen		
Title of the thesis:	Quantum Transport in the Ballistic and Coulomb Blockade Regimes		
Date:	5th September 2003	**Number of pages:**	94
Department:	Electrical and Communications Engineering		
Professorship:	Computational Engineering	**Code:**	S-114
Supervisor:	Jukka Tulkki		
Instructor:	Jukka Tulkki		

The first part of this master's thesis reviews computational methods for conductance calculations in the ballistic transport regime. Detailed conductance calculations based on the mode matching and recursive Green's function methods are carried out for selected two-dimensional (2D) and three-dimensional (3D) conducting channels. The calculations are performed at zero and non-zero temperatures and they are focused into the linear transport regime where the difference of the chemical potential of the electron reservoirs is small (low bias voltage). Furthermore the mode matching method was applied to calculations of 3D conductance of a silicon quantum point contact (QPC). The calculated conductances of Si QPC agree qualitatively with measured results.

The second part of this master's thesis deals with the Coulomb blockade and single charge tunneling effects. Simulation of single electron transistor (SET) and SET circuits are performed. Furthermore the Monte Carlo (MC) method for single electron circuit simulations is discussed. As an application the structure and function of a multigate SET based exclusive or (XOR) gate is presented.

Keywords: conductance, mode matching method, recursive Green's function method, single electron transistor

TEKNILLINEN KORKEAKOULU

DIPLOMITYÖN TIIVISTELMÄ

Tekijä:	Teppo Häyrynen	
Työn aihe:	Elektronikuljetus ballistisella ja Coulombin saarron alueilla	
Päivämäärä:	5. syyskuuta 2003	**Sivumäärä:** 94
Osasto:	Sähkö- ja tietoliikennetekniikan osasto	
Professuuri:	Laskennallinen tekniikka	**Koodi:** S-114
Työn valvoja:	Jukka Tulkki	
Työn ohjaaja:	Jukka Tulkki	

Tämän diplomityön ensimmäinen osa käsittelee konduktanssin laskemista ballistisella alueella nollalämpötilassa ja nollaa suuremmissa lämpötiloissa. Mode matching sekä rekursiivisen Greenin funktio -menetelmien soveltaminen valittujen kaksi- (2D) ja kolmiuloitteisten (3D) kanavien konduktanssien laskemiseen on esitetty yksityiskohtaisesti. Konduktanssilaskut on suoritettu lineaarisella alueella eli pienillä bias-jänitteen arvoilla. Lisäksi mode matching -menetelmällä laskettu piistä valmistetun (3D) kvanttipistekontaktin (QPC) konduktanssikuvaaja vastaa muodoltaan mitattuja tuloksia.

Työn jälkimmäisessä osassa kuvataan Coulombin saarto -ilmiö sekä yhden elektronin transistorin (SET) rakenne ja toiminta. Lisäksi Monte Carlo (MC) -menetelmän käyttö SET piirien mallintamiseen ja simulointituloksia on esitetty. Esimerkkisovelluksena on esitetty monihila-SET:iin perustuvan loogisen ehdoton tai (XOR) -portin rakenne ja toiminta.

Avainsanat:	konduktanssi, mode matching -menetelmä, rekursiivinen Greenin funktio -menetelmä, yhden elektronin transistori

Contents

Symbols and Abbreviation

$\hat{a}_\mu$	annihilation operator
$\hat{a}_\mu^\dagger$	creation operator
B	magnetic flux density
C	capacitance
E	electric field
e	elemental electric charge
$f(\mathcal{E})$	Fermi-Dirac distribution function
G	conductance
$\mathbf{G}(\mathbf{r}, \mathbf{r}', \mathcal{E})$	Green's function
GSM	generalized scattering matrix
$\mathcal{H}$	Hamiltonian operator
h	Planck's constant
$\hbar$	reduced Planck's constant
I	current
J	current density
$\mathbf{k}$	wavevector
k_B	Boltzmann constant
l.h.s.	left-hand side
m_0	electron rest mass
m^*	effective mass
$N(\mathcal{E})$	density of states function
$\hat{N}$	number operator
$p(n, t)$	time dependent probability

Q	charge
QPC	quantum point contact
R	resistance
R_T	tunneling resistance
r.h.s.	right-hand side
S	scattering matrix
SET	single electron transistor
T	transmission probability, absolute temperature
$u_{n\mathbf{k}}(\mathbf{r})$	periodic part of Bloch's function
V	voltage, potential energy
v_F	Fermi velocity
$\Gamma(\Delta\mathcal{E})$	transition rate
δ_{nm}	Dirac's delta function
$\mathcal{E}$	energy
ε	dielectric constant
λ_F	Fermi wavelength
μ	chemical potential
ρ	resistivity
σ	conductivity
τ	time
ϕ	potential
$\phi(\mathbf{r})$	wave function
$\Psi(\mathbf{r})$	wave function
$\psi(\mathbf{r})$	wave function
$\|\phi\rangle$	ket-vector
$\langle\phi\|$	bra-vector

Chapter 1

Introduction

In mesoscopic conductors the transport of electrons is limited to channels having a diameter of few to few tens of atom sizes. There are three different length scales that characterize mesoscopic systems:

1. The de Broglie wavelength: $\lambda = h/p = 2\pi/k$.

2. The mean free path which is the average distance that an electron travels before being scattered into a different wavevector direction i.e. its initial momentum is destroyed. It is defined as $\Lambda = v_F\tau$ [1], where v_F is the Fermi velocity and τ is the relaxation time.

3. The phase relaxation length, which is the average distance that an electron travels before its initial phase is destroyed, is $l_\phi = \Lambda\sqrt{\tau_\phi/\tau}$ [1], where τ_ϕ is the phase relaxation time.

These length scales are material and temperature dependent and also an external electro-magnetic field has an affect on them. The relation of system size L and mean free path Λ divides the transport into the ballistic and diffusive transport regimes. The transport of the electrons is ballistic if $L \ll \Lambda$ and it is diffusive if $L \gg \Lambda$. On the other hand the phase relaxation length is associated with inelastic scattering. The phase of an electron can be destroyed e.g. by scattering from other electrons or lattice vibrations.

A mesoscopic system can be roughly categorized depending on the relative magnitude of the dimensions of the device (a system is confined into a box with sizes L_x, L_y and L_z) and the Fermi wavelength $\lambda_F = 2\pi/k_F$ as follows [1]:

(i)	$\lambda_F \ll L_x, L_y, L_z$	:	3D (bulk)
(ii)	$\lambda_F \sim L_x < L_y, L_z$	:	quasi 2D (thin films)
(iii)	$L_x < \lambda_F \ll L_y, L_z$	:	2D (MOSFETs)
(iv)	$L_x < L_y \sim \lambda_F \ll, L_z$	:	quasi 1D (quantum wires)
(v)	$L_x, L_y < \lambda_F \ll, L_z$	:	1D
(vi)	$L_x, L_y, L_z < \lambda_F$	:	0D (quantum dots).

1.1 Drude Model

The Drude model is based on the ideal gas approximation, where the energy distribution of electrons follows Boltzmann statistics. The Drude model was developed to explain the microscopic details of macroscopic experiments of current flow, heat flow and effects of magnetic field in a phenomenological way.

The current in metals is described by the Ohm's law

$$I = \frac{1}{R}V, \tag{1.1}$$

where the resistance R depends on the length of the wire L, on the cross-section area of the wire A and on the resistivity of the material ρ. Thus it is reasonable to write the Ohm's law by using the electric field E and the current density J as follows

$$J = \frac{1}{\rho}E = \sigma E, \tag{1.2}$$

where the relations $V = EL$, $R = \rho L/A$ and $I = JA$ has been used and σ denotes the conductivity of the material. In the Drude model it is assumed that free electrons collide with immobile positive ions on an average when a time τ has elapsed after previous collision. Furthermore, between

these collisions electrons are assumed to move without any interaction with the ions or other electrons. Since it is also assumed that immediately after collisions electrons have the velocity corresponding to the thermo-dynamical equilibrium at certain temperature, the average velocity $\mathbf{v}$ is zero at zero field. Thus the average velocity in an external electric field can be obtained directly from Newton's equation of motion

$$\mathbf{v}_{ave} = -\frac{e\mathbf{E}\tau}{m}. \tag{1.3}$$

According to classical electromagnetism the current density in an applied electric field can be represented by using the electron density, the average velocity of electrons and the elemental electric charge:

$$\mathbf{J} = -ne\mathbf{v}. \tag{1.4}$$

Now by substituting the velocity given in equation (1.3) into the current density (1.4) we get

$$J = \frac{ne^2\tau}{m}E. \tag{1.5}$$

Comparing this to equation (1.2) we obtain the conductivity

$$\sigma = \frac{ne^2\tau}{m}. \tag{1.6}$$

The average time between collisions can be estimated from measured conductivity or resistivity. The mean free path, which is the distance traveled by an electron between two subsequent collisions, can be calculated by using τ and the thermodynamic equilibrium velocity [2]

$$\frac{1}{2}mv^2 = \frac{3}{2}k_BT \tag{1.7}$$

and it is given by

$$l = v\tau. \tag{1.8}$$

The order of magnitude values of the relaxation time, Fermi velocity, the mean free path and the conductivity in metals are $10^{-14}\ s$, $10^6\ m/s$, $10^{-9}\ m$ and $10^8\ 1/(\Omega m)$ [3, 4], respectively.

1.1.1 Hall Effect

In the Hall experiment we consider a wire with a current flowing through it. Let the current flow into x-direction and the applied magnetic field to be perpendicular to the wire, say into z-direction, as shown in figure 1.1. The magnetic field causes a Lorentz force on free moving charged particles. This force drives electrons into negative y-direction leaving positive charge on the opposite side. The oppositely charged edges of the conductor produce an electric field $\mathbf{E_y}$ parallel to negative y-direction. The charge separation continues to grow until the transverse forces caused by the electric and magnetic fields cancel each other.

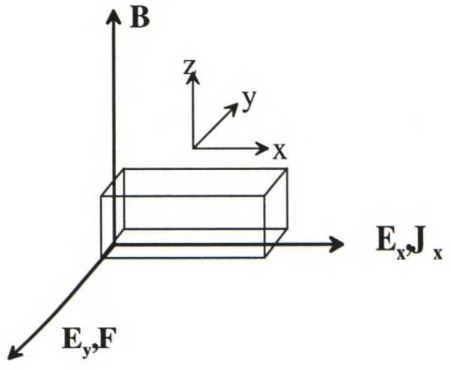

Figure 1.1: Relative directions of the magnetic and electric fields and the Lorentz force in a conductor.

The Hall effect is associated with two characteristic quantities. One is the magneto-resistance [2]

$$\rho = \frac{E_x}{J_x} \tag{1.9}$$

and the other is the Hall coefficient [3, 5]

$$R_H = \frac{E_y}{J_x|B|} = -\frac{1}{ne}, \tag{1.10}$$

where B is the magnetic flux density, and n is the electron density. Relations (1.9) and (1.10) can be derived from the Drude model. The important re-

sults are (1) that the magneto-resistance is independent of the magnetic flux density and (2) that the Hall factor depends only on the electron density.

1.2 Quantum Mechanical Treatment of Electrons

The eigenstates of electrons are solutions of the (time independent) Schrödinger equation

$$\Big[-\frac{\hbar^2}{2m}\Big(\frac{\partial^2}{\partial x^2}+\frac{\partial^2}{\partial y^2}+\frac{\partial^2}{\partial z^2}\Big)+V(x,y,z)\Big]\Psi(x,y,z)=\mathcal{E}\Psi(x,y,z). \quad (1.11)$$

For free electrons the potential energy is zero; $V(x,y,z)=0$. In this case the general solution of the Schrödinger equation is given by

$$\Psi(\mathbf{r})=\frac{1}{\sqrt{L^3}}e^{i\mathbf{k}\cdot\mathbf{r}}. \quad (1.12)$$

The L^3 in equation (1.12) represents the volume of the conductor and it is included for the purpose of normalization: $\int_{L^3}|\Psi(\mathbf{r})|\mathrm{d}^3r=1$.

There are two kind of possible boundary conditions for $\Psi(\mathbf{r})$ corresponding to the physical conditions that we want to examine. For the standing wave solutions the wavefunction is zero at the boundaries and for the propagating electrons the periodic boundary conditions are used. In the first case the solutions of wavefunction are sine or cosine and the allowed values for k are

$$k_i=\frac{\pi}{L},\frac{2\pi}{L},\frac{3\pi}{L},\ldots, \quad i=x,y,z. \quad (1.13)$$

In the latter case the periodic boundary conditions require that

$$\Psi(x+L,y,z)=\Psi(x,y+L,z)=\Psi(x,y,z+L)=\Psi(x,y,z), \quad (1.14)$$

which yield to following allowed values for k

$$k_i=\frac{2\pi n_i}{L}, \quad i=x,y,z, \qquad n_i\in\mathbf{Z}, \quad (1.15)$$

where k has an cut of at the boundary of Brillouin zone. The volume that each electronic state takes in the k-space is $(2\pi/L)^3$ in both cases.

1.2.1 Density of States

The density of states (DOS) $N(\mathcal{E})$ gives the number of electronic states per unit volume and unit energy around the energy $\mathcal{E}$. The number of states per unit volume in the energy interval $\mathcal{E}$, $\mathcal{E} + \mathrm{d}\mathcal{E}$ is $N(\mathcal{E})\mathrm{d}\mathcal{E}$. Wavefunction for free electrons was given in equation (1.12) as a solution of Schrödinger equation. Corresponding energy eigenvalues obey the parabolic relation

$$\mathcal{E} = \frac{\hbar^2 k^2}{2m} \tag{1.16}$$

from which we get

$$k = \sqrt{\frac{2m\mathcal{E}}{\hbar^2}} \tag{1.17}$$

$$\mathrm{d}k = \frac{1}{2}\Big(\frac{2m}{\hbar^2}\Big)^{\frac{1}{2}} \frac{\mathrm{d}\mathcal{E}}{\sqrt{\mathcal{E}}}. \tag{1.18}$$

In three-dimensional (3D) case the volume between k and $k + \mathrm{d}k$ in the k-space is a volume of a spherical shell $\Delta V = 4\pi k^2 \mathrm{d}k$. Similarly in 2D and 1D the area and the length between k and $k + \mathrm{d}k$ are $\Delta A = 2\pi k \mathrm{d}k$ and $\Delta L = 2\mathrm{d}k$, respectively. The number of states between k and $k + \mathrm{d}k$ is the total space between k and $k + \mathrm{d}k$ divided by the space of one state. Thus the number of states per unit energy and unit volume, area or length are

$$N_{3D}(\mathcal{E}) = \frac{2}{V}\frac{4\pi k^2}{(2\pi)^3/V}\frac{\mathrm{d}k}{\mathrm{d}\mathcal{E}} = \frac{k^2}{\pi^2}\frac{\mathrm{d}k}{\mathrm{d}\mathcal{E}} \tag{1.19}$$

$$N_{2D}(\mathcal{E}) = \frac{2}{A}\frac{2\pi k}{(2\pi)^2/A}\frac{\mathrm{d}k}{\mathrm{d}\mathcal{E}} = \frac{k}{\pi}\frac{\mathrm{d}k}{\mathrm{d}\mathcal{E}} \tag{1.20}$$

$$N_{1D}(\mathcal{E}) = \frac{2}{L}\frac{2}{(2\pi)/L}\frac{\mathrm{d}k}{\mathrm{d}\mathcal{E}} = \frac{2}{\pi}\frac{\mathrm{d}k}{\mathrm{d}\mathcal{E}}, \tag{1.21}$$

where the factor of two is included because of spin degeneracy. Now by substituting equation (1.18) into above equations we get the density of states functions

$$N_{3D}(\mathcal{E}) = \frac{1}{2\pi^2}\Big(\frac{2m}{\hbar^2}\Big)^{\frac{3}{2}}\sqrt{\mathcal{E}} \tag{1.22}$$

$$N_{2D}(\mathcal{E}) = \frac{1}{2\pi}\Big(\frac{2m}{\hbar^2}\Big) \tag{1.23}$$

$$N_{1D}(\mathcal{E}) = \frac{1}{\pi}\Big(\frac{2m}{\hbar^2}\Big)^{\frac{1}{2}}\frac{1}{\sqrt{\mathcal{E}}}. \tag{1.24}$$

1.2.2 Electron Density

In quantum mechanics particles are divided into two categories according to their spin angular momentum quantum number. For bosons like photons and phonons the spin quantum number is an integer and for fermions like electrons, protons and neutrons the spin quantum number is an odd multiple of an half.

According to the Pauli exclusion principle only one fermion can occupy one quantum state. It follows that the energy distribution which minimizes the free energy of the system is the Fermi-Dirac distribution

$$f(\mathcal{E}) = \frac{1}{e^{\frac{\mathcal{E}-\mu}{k_B T}} + 1}. \tag{1.25}$$

The chemical potential μ is defined as [6]:

$$\mu = \left(\frac{\partial U}{\partial \mathrm{n}}\right)_{V,S}, \tag{1.26}$$

where n is the number of particles, V is the volume and S is the entropy. Thus the chemical potential shows how much the internal energy changes when one electron is added to the system without changing its thermodynamical state.

By using Fermi-Dirac distribution function the electron density and the total energy of an electron gas can be calculated from

$$n = \int_0^\infty N(\mathcal{E}) f(\mathcal{E}) \mathrm{d}\mathcal{E} \tag{1.27}$$

and

$$\mathcal{E}_{tot} = \int_0^\infty \mathcal{E} N(\mathcal{E}) f(\mathcal{E}) \mathrm{d}\mathcal{E}. \tag{1.28}$$

At zero temperature ($T = 0\mathrm{K}$) it follows from equation (1.27) that $\mu = \mathcal{E}_F = \frac{\hbar^2}{2m}(3\pi^2 n)^{\frac{2}{3}}$, which corresponds to Fermi wave-vector $k_F = (3\pi^2 n)^{\frac{1}{3}}$ and Fermi velocity $v_F = \frac{\hbar}{m}(3\pi^2 n)^{\frac{1}{3}}$.

1.3 Effective Mass Theory

1.3.1 Bloch's Theorem

The Bloch's theorem generates a model for description of electrons in a periodic potential structure like a crystal. According to Bloch's theorem the solutions of the Schrödinger equation in a periodic potential are products of a plane wave $e^{i\mathbf{k}\cdot\mathbf{r}}$ and a periodic function $u_{n\mathbf{k}}(\mathbf{r})$ with the latter having the same periodicity as the crystal potential. Therefore the eigenfunctions can be written as [3, 2]:

$$\Psi_{n\mathbf{k}}(\mathbf{r}) = e^{i\mathbf{k}\cdot\mathbf{r}} u_{n\mathbf{k}}(\mathbf{r}), \tag{1.29}$$

where $u_{n\mathbf{k}}(\mathbf{r}+\mathbf{R}) = u_{n\mathbf{k}}(\mathbf{r})$ if $\mathbf{R}$ is the lattice vector.

By substituting Bloch's functions into Schrödinger equation and dividing by the plane wave part gives

$$\begin{aligned} &-\frac{\hbar^2}{2m}\nabla_{\mathbf{r}}^2 u_{n\mathbf{k}}(\mathbf{r}) - \frac{i\hbar^2 k}{m}\nabla_{\mathbf{r}} u_{n\mathbf{k}}(\mathbf{r}) + \Big[\frac{\hbar^2 k^2}{2m} + V(\mathbf{r})\Big] u_{n\mathbf{k}}(\mathbf{r}) \\ &= \mathcal{E} u_{n\mathbf{k}}(\mathbf{r}), \end{aligned} \tag{1.30}$$

which depends also on k. Thus the eigenfunctions and eigenenergies are functions of k and furthermore there exist multiple solutions for each value of k, indexed with n. Therefore the eigenfunctions has been written as:

$$\Psi_{n\mathbf{k}}(\mathbf{r}) = e^{i\mathbf{k}\cdot\mathbf{r}} u_{n\mathbf{k}}(\mathbf{r}). \tag{1.31}$$

The eigenenergies are given by

$$\mathcal{E} \equiv \mathcal{E}_n(\mathbf{k}). \tag{1.32}$$

1.3.2 Semiclassical Equations of Motion

The group velocity of a wave-packet is defined as

$$\mathbf{v}_g = \frac{\mathrm{d}\omega}{\mathrm{d}\mathbf{k}}. \tag{1.33}$$

Because the wave-packet corresponds to a classical particle, the velocity of a particle can be derived from above equation by using relation $\mathcal{E} = \hbar\omega$ as follows:

$$\mathbf{v} = \frac{1}{\hbar}\frac{\mathrm{d}\mathcal{E}(\mathbf{k})}{\mathrm{d}\mathbf{k}} = \frac{1}{\hbar}\nabla_{\mathbf{k}}\mathcal{E}(\mathbf{k}). \tag{1.34}$$

From Newton's second law of motion $\mathrm{d}\mathbf{p}/\mathrm{d}t = \mathbf{F}$ we get

$$\hbar\frac{\mathrm{d}\mathbf{k}}{\mathrm{d}t} = -q(\mathbf{E} + \mathbf{v} \times \mathbf{B}), \tag{1.35}$$

where relations $\mathbf{p} = \hbar\mathbf{k}$ and Lorentz force have been used. The acceleration is obtained from equation (1.34) by derivating:

$$\mathbf{a} = \frac{\mathrm{d}\mathbf{v}}{\mathrm{d}t} = \frac{1}{\hbar}\nabla_{\mathbf{k}}\nabla_{\mathbf{k}}\mathcal{E}(\mathbf{k})\frac{\mathrm{d}\mathbf{k}}{\mathrm{d}t} \tag{1.36}$$

$$= \frac{1}{\hbar^2}\nabla_{\mathbf{k}}\nabla_{\mathbf{k}}\mathcal{E}(\mathbf{k}) \cdot (-q)[\mathbf{E} + \mathbf{v} \times \mathbf{B}] = \frac{1}{m^*}\mathbf{F}. \tag{1.37}$$

The effective mass is then obtained from above equation as follows

$$\frac{1}{m^*} = \frac{1}{\hbar^2}\nabla_{\mathbf{k}}\nabla_{\mathbf{k}}\mathcal{E}(\mathbf{k}). \tag{1.38}$$

1.3.3 Envelope Function Approximation

Calculations of the electronic structure in semiconductors can be done by using $\mathbf{k} \cdot \mathbf{p}$ or effective mass theory, which assumes a parabolic carrier dispersion relation $\mathcal{E} = \hbar^2k^2/(2m^*)$. The effective mass method is a reasonable approximation close to the band edges. Most optical and electronic devices operate in this regime. In the effective mass theory the periodic crystal potential is accounted for trough the effective mass

$$m^* = \hbar^2 \Big/ \frac{\mathrm{d}^2\mathcal{E}(\mathbf{k})}{\mathrm{d}\mathbf{k}^2}. \tag{1.39}$$

For materials which have anisotropic equal energy surfaces equation (1.38) must be generalized for the effective mass tensor as follows [5]:

$$\frac{1}{m^*_{ij}} = \frac{1}{\hbar^2}\frac{\mathrm{d}^2\mathcal{E}(\mathbf{k})}{\mathrm{d}\mathbf{k}_i\mathrm{d}\mathbf{k}_j}, \tag{1.40}$$

where i, j are Cartesian coordinates. In the bulk semiconductor the wavefunction has the Bloch form (1.29), where the rapidly varying periodic crystal potential part $u_{n\mathbf{k}}(\mathbf{r})$ is modulated by a slowly varying plane wave $e^{i\mathbf{k}\cdot\mathbf{r}}$. The multiband $\mathbf{k}\cdot\mathbf{p}$ method accounts for mixing of the zeroth order states. The multiband wavefunction is given by $\sum_n c_n(\mathbf{k})e^{i\mathbf{k}\cdot\mathbf{r}}u_{n0}(\mathbf{r})$, where the sum is taken over the leading conduction and valence bands and $c_n(\mathbf{k})$ are the weight factors, which are obtained by diagonalizing the multiband Hamiltonian for fixed $\mathbf{k}$.

In a heterostructure two approximately lattice matched III-V compound semiconductor materials M_I and M_{II} having different bandgaps but the same crystal symmetry form an abrupt heterointerface. The interface causes a discontinuity in the conduction and valence band edges. As an example we consider a simple quantum well shown in figure 1.2. This corresponds to

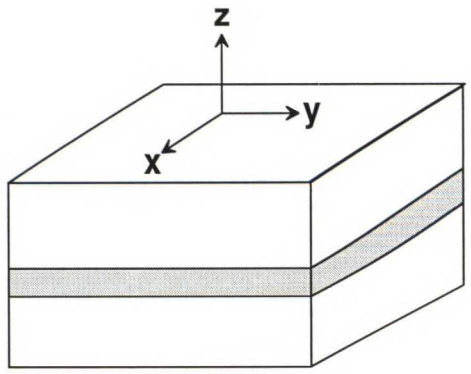

Figure 1.2: A schematic picture of quantum well: a narrow layer of well material (M_{II}) (shaded area in the figure) is between bulk material (M_I).

a structure where an external one-dimensional potential $\mathcal{E}_{\text{pot}}(z)$ is added to the crystal potential $\mathcal{E}_{\text{cry}}(\mathbf{r})$ of the bulk material in order to account for the band edge discontinuity. Therefore the heterostructure can be described by Schrödinger equation

$$\mathcal{H}\Psi(\mathbf{r}) = [-\frac{\hbar^2\nabla^2}{2m_0} + \mathcal{E}_{\text{cry}}(\mathbf{r}) + \mathcal{E}_{\text{pot}}(z)]\Psi(\mathbf{r}) = \mathcal{E}\Psi(\mathbf{r}), \tag{1.41}$$

where $\mathcal{E}$ is the energy eigenvalue. The plane wave motion normal to the plane of the interface is not affected by the 1D heterostructure potential $\mathcal{E}_{\text{pot}}(z)$. By assuming that the atomic Bloch states at Γ point are continuous across the interface: $u_{n0}^{M_I}(\mathbf{r}) = u_{n0}^{M_{II}}(\mathbf{r})$ for all strongly coupled valence and conduction bands n, the wavefunction in either material can be expressed as weighted sum of atomic Bloch states $u_{n0}(\mathbf{r})$ as follows [7]:

$$\Psi(\mathbf{r}) = \sum_n u_{n0}(\mathbf{r}) e^{i\mathbf{k}_{\|}\cdot\mathbf{r}} F_n(z), \tag{1.42}$$

where $\mathbf{k}_{\|}$ is the wavevector in the interface plane and $F_n(z)$ is the envelope function. In analogy to the $\mathbf{k}\cdot\mathbf{p}$ theory equation (1.42) is a good approximation close to the band edges: $|k_x|, |k_y| \ll 4\pi/a$, where a is the lattice constant. If the band coupling is neglected, inserting equation (1.42) into equation (1.41) leads to Schrödinger like equations for the envelope functions $F_n(z)$. These are called as the envelope Schrödinger equations and they can be written as

$$[-\frac{\hbar^2}{2m_0}\frac{\mathrm{d}^2}{\mathrm{d}z^2} + \mathcal{E}_p(z)]F_n(z) = \mathcal{E}F_n(z), \tag{1.43}$$

where the electron mass is still equal to the rest mass. It can be shown that if the coupling with other bands is included the rest mass in equation (1.43) has to be replaced by the position dependent effective mass. The calculations done in chapters 4 5 excludes the band coupling.

1.3.4 Effective Mass in Silicon

In bulk silicon the indirect conduction band consists of six equivalent anisotropic valleys in the k-space. These anisotropic valleys have minima on the [100], [010] and [001] axes. The distances of the minima measured from the Γ-point are denoted by $a \approx 10^{10}$ m^{-1}. The minima are located at $[\pm a, 0, 0]$, $[0, \pm a, 0]$ and $[0, 0, \pm a]$. The equipotential energy surfaces of these minima or valleys have a shape of a rotational ellipsoid. The axis of rotation coincides with the axis on which the valley is located. These valleys are characterized by two

different effective masses, the longitudinal effective mass and the transverse effective mass. The longitudinal mass corresponds to motion in the direction of the axis of rotation and the transverse mass corresponds to motion orthogonal to the axis of rotation (see figure 1.3). In these valleys the longitudinal effective mass is $m_l^* = 0.98m_0$ and the transverse effective mass is $m_t^* = 0.19m_0$ along equivalent $\langle 100 \rangle$ directions.

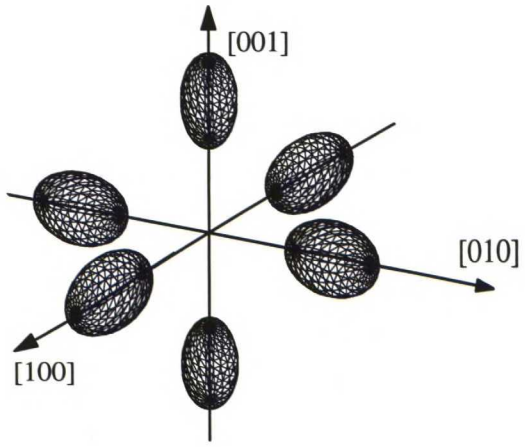

Figure 1.3: Six constant energy ellipsoids for electrons in silicon with $m_t^* = 0.19m_0$ and $m_l^* = 0.98m_0$.

Let us assume that there is a quantum wire on the xy-plane and it forms an angle θ counterclockwise with y-axis, so we have rotated the x- and y-axes counterclockwise around the z-axis by θ. We can write the effective mass Schrödinger equation for each six valleys on rotated coordinates as follows [8]:

$$\Big[-\frac{\hbar^2}{2m_x^*}\frac{\partial^2}{\partial x^2} - \frac{\hbar^2}{2m_z^*}\frac{\partial^2}{\partial z^2} + V(x,z) \Big] \Psi(x,z) = \mathcal{E}\Psi(x,z). \tag{1.44}$$

We have three separate cases [8]:

1. For the $[0, 0, \pm a]$ valleys effective masses are

$$m_x^* = m_t^* = 0.19m_0$$

$$\begin{aligned} m_y^* &= m_t^* = 0.19 m_0 \\ m_z^* &= m_l^* = 0.98 m_0 \end{aligned}$$

2. For the $[0, \pm a, 0]$ valleys effective masses are

$$\begin{aligned} m_x^* &= \left[\frac{\cos^2 \theta}{m_t^*} + \frac{\sin^2 \theta}{m_l^*} \right]^{-1} \\ m_y^* &= m_l^* \cos^2 \theta + m_t^* \sin^2 \theta \\ m_z^* &= m_t^* \end{aligned}$$

3. For the $[\pm a, 0, 0]$ valleys effective masses are

$$\begin{aligned} m_x^* &= \left[\frac{\sin^2 \theta}{m_t^*} + \frac{\cos^2 \theta}{m_l^*} \right]^{-1} \\ m_y^* &= m_l^* \sin^2 \theta + m_t^* \cos^2 \theta \\ m_z^* &= m_t^*. \end{aligned}$$

Chapter 2

Conductance

2.1 Ballistic Transport

Let us consider a device where a conductor connects two electron reservoirs. In the ballistic transport approach it is assumed that particles move trough this channel region without scattering. This assumption holds true if the relative magnitude of the mean free path Λ and the system size L is such that $L \ll \Lambda$. The conductor region is modeled by transmission and reflection of

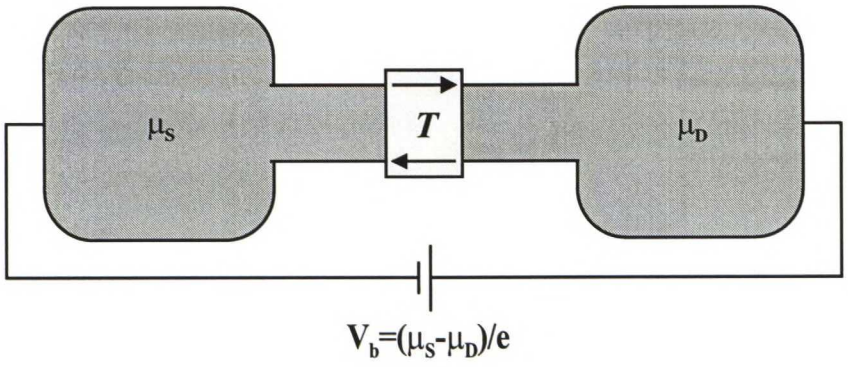

Figure 2.1: A scatterer is connected to electron reservoirs with ideal leads. The bias voltage $eV_b = \mu_S - \mu_D$ separates the chemical potentials of the reservoirs.

the incoming waves at the contacts of conductor and reservoirs. Let reservoirs

have different Fermi levels $\mathcal{E}_{F1}$ and $\mathcal{E}_{F2}$ separated with a small bias voltage V_b. Then $\mathcal{E}_{F1} = \mathcal{E}_{F2} + eV_b$. The current is carried only by electrons which flow from occupied states in the source reservoir into unoccupied states in the drain reservoir. At zero temperature the current is carried by the electrons with energies between $\mathcal{E}_{F2}$ and $\mathcal{E}_{F1}$ since each state below the Fermi energy is occupied and each state above Fermi level is empty. On the contrary at nonzero temperatures the Fermi-Dirac distribution function has to be used: The initial state is occupied with the probability $f_i(\mathcal{E})$ and the final state is unoccupied with the probability $1 - f_f(\mathcal{E})$.

2.2 Two-Terminal Conductance

Let us consider a case where a scatterer is connected at both ends to electron reservoirs with ideal leads. Also the electron reservoirs are assumed to be ideal so that they satisfy the following conditions [9]:

1. The reservoirs are in equilibrium with a given electrochemical potential μ_i (which is different for the various reservoirs attached to the conductor).

2. They are large enough such that the currents flowing in or out are negligible deep within the reservoirs (i.e. they stay in equilibrium with unchanged μ_i even in the presence of the current flow).

3. Electrons entering the reservoirs are not reflected back into the conductor before equilibration.

Let μ_S and μ_D represent the chemical potentials at the source and drain reservoirs, respectively, and $eV_b = \mu_S - \mu_D$ (see figures 2.1 and 2.2). At zero temperature with a negligible bias voltage the conductance is given by the Landauer formalism [10, 11, 9]:

$$G = \frac{2e^2}{h}T, \tag{2.1}$$

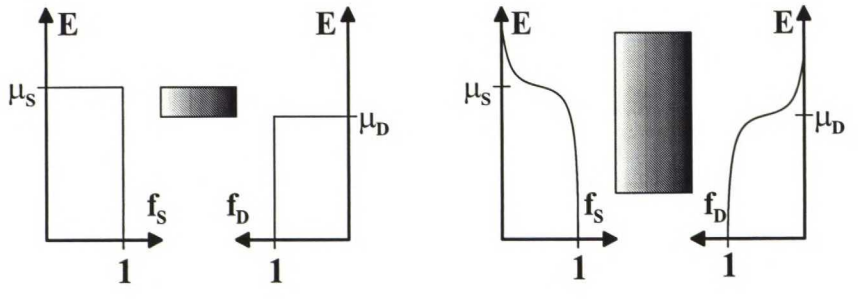

Figure 2.2: Left: Schematic picture of the energy distributions of figure 2.1 at zero temperature. Right: The same at nonzero temperature. The shaded areas represent the conducting energy channels in the conductor.

where T denotes the total transmission through the scatterer (i.e. the sum of the transmission probability of all conducting channels) at the Fermi energy.

On the contrary at the nonzero temperatures the energy distribution of electrons must be taken into account and the situation becomes more subtle. The influx of electrons per unit energy from an ideal source lead can be written by using the velocity of electrons v, the density of states function $N(\mathcal{E})$[1], the Fermi-Dirac distribution $f_i(\mathcal{E}) = \left(1 + e^{\frac{\mathcal{E}-\mu_i}{k_B T}}\right)^{-1}$ and the transmission coefficient:

$$\begin{aligned} i^+(\mathcal{E}) &= \frac{1}{2} \cdot e \cdot v \cdot N(\mathcal{E}) \cdot f_S(\mathcal{E}) \cdot T(\mathcal{E}) \\ &= \frac{1}{2} \cdot e \cdot v \cdot \frac{2}{\pi\hbar v} \cdot f_S(\mathcal{E}) \cdot T(\mathcal{E}) \\ &= \frac{2e}{h} f_S(\mathcal{E}) T(\mathcal{E}), \end{aligned} \tag{2.2}$$

where the factor $\frac{1}{2}$ is included because we take into account only those states that corresponds to electrons propagating to right. Similarly the influx form ideal drain lead is given by

$$i^-(\mathcal{E}) = \frac{2e}{h} f_D(\mathcal{E}) T(\mathcal{E}). \tag{2.3}$$

[1] $N(\mathcal{E}) = \frac{1}{\pi\hbar}\sqrt{\frac{2m}{\mathcal{E}}} = \frac{2}{\pi\hbar}\sqrt{\frac{m}{2\mathcal{E}}} = \frac{2}{\pi\hbar v}$

The total current trough the wire is obtained by integrating the difference $i^+(\mathcal{E}) - i^-(\mathcal{E})$ over the relevant energy range:

$$I = \frac{2e}{h} \int_{\mu_D - nk_BT}^{\mu_S + nk_BT} T(\mathcal{E})(f_S(\mathcal{E}) - f_D(\mathcal{E}))\mathrm{d}\mathcal{E}, \tag{2.4}$$

where n is a positive constant stating that the relevant energy range is a few k_BTs around the chemical potentials.

In equation (2.4) it is assumed that the transmission coefficient for electrons propagating from left to right is equal to the transmission coefficient for the electrons which are propagating from right to left. That assumption holds true if there is no inelastic scattering inside the device. Finally the conductance can be calculated when the current and the applied bias voltage are known:

$$G = \frac{I}{V_b} = \frac{2e^2}{h(\mu_S - \mu_D)} \int_{\mu_D - nk_BT}^{\mu_S + nk_BT} T(\mathcal{E})(f_S(\mathcal{E}) - f_D(\mathcal{E}))\mathrm{d}\mathcal{E}. \tag{2.5}$$

At the linear transport regime it is assumed that $eV_b = \mu_S - \mu_D$ is very small. Thus we can write as a good approximation:

$$\begin{aligned} \lim_{V_b \to 0} \frac{f_S(\mathcal{E}) - f_D(\mathcal{E})}{\mu_S - \mu_D} &= -\lim_{V_b \to 0} \frac{f_S(\mathcal{E} + eV_b) - f_S(\mathcal{E})}{eV_b} \\ &= -\frac{\partial f_S(\mathcal{E})}{\partial \mathcal{E}}. \end{aligned} \tag{2.6}$$

Hence the conductance can be written as follows:

$$G = \frac{2e^2}{h} \int_{\mu_D - nk_BT}^{\mu_S + nk_BT} T(\mathcal{E})\Big(-\frac{\partial f_S(\mathcal{E})}{\partial \mathcal{E}}\Big)\mathrm{d}\mathcal{E}. \tag{2.7}$$

Thus, if V_b is very small, it follows from equations (2.5) and (2.7) that the conductance is independent of the bias voltage V_b and that the current depends linearly on it.

Although it is sufficient to assume that $\mu_S - \mu_D$ is very small for the current to depend linearly on the bias voltage this is not a necessary condition. We will next derive the necessary condition for linear relationship between the

current and the applied bias voltage. Let us write

$$\begin{aligned} f_S(\mathcal{E}) - f_D(\mathcal{E}) &= -\int_{\mu_D}^{\mu_S} \frac{-e^{(\mathcal{E}-\mu)/(k_BT)}}{(1+e^{(\mathcal{E}-\mu)/k_BT})^2} \mathrm{d}\mu \\ &= \int_{\mu_D}^{\mu_S} \Big[\frac{\partial}{\partial\mu}\big(1+e^{(\mathcal{E}-\mu)/(k_BT)}\big)^{-1}\Big]\mathrm{d}\mu \\ &= \int_{\mu_D}^{\mu_S} \Big[-\frac{\mathrm{d}}{\mathrm{d}(\mathcal{E}-\mu)}\frac{1}{1+e^{(\mathcal{E}-\mu)/(k_BT)}}\Big]\mathrm{d}\mu \\ &= \int_{\mu_D}^{\mu_S} \Big[-\frac{\mathrm{d}}{\mathrm{d}\mathcal{E}}\frac{1}{1+e^{(\mathcal{E}-\mu)/(k_BT)}}\Big]\mathrm{d}\mu \\ &= \int_{\mu_D}^{\mu_S} F(\mathcal{E}-\mu)\mathrm{d}\mu, \end{aligned} \tag{2.8}$$

where

$$F(\mathcal{E}) \equiv \frac{\mathrm{d}}{\mathrm{d}\mathcal{E}}\frac{1}{1+e^{\mathcal{E}/(k_BT)}}. \tag{2.9}$$

Thus the current in equation (2.4) can be rewritten as

$$\begin{aligned} I &= \frac{2e}{h}\int T(\mathcal{E})[f_S(\mathcal{E}) - f_D(\mathcal{E})]\mathrm{d}\mathcal{E} \\ &= \frac{2e}{h}\int T(\mathcal{E})\Big(\int_{\mu_D}^{\mu_S} F(\mathcal{E}-\mu)\mathrm{d}\mu\Big)\mathrm{d}\mathcal{E} \\ &= \int_{\mu_D}^{\mu_S}\Big(\frac{2e}{h}\int T(\mathcal{E})F(\mathcal{E}-\mu)\mathrm{d}\mathcal{E}\Big)\mathrm{d}\mu. \end{aligned} \tag{2.10}$$

By comparing the above result with the current formula

$$I = GV_b = G\frac{\mu_S - \mu_D}{e} \tag{2.11}$$

it is seen that in the linear transport regime the conductance is given by

$$\begin{aligned} G = G(\mu) &= \frac{2e^2}{h}\int T(\mathcal{E})F(\mathcal{E}-\mu)\mathrm{d}\mathcal{E} \\ &= \frac{2e^2}{h}\int T(\mathcal{E})\Big[-\frac{\mathrm{d}}{\mathrm{d}\mathcal{E}}\frac{1}{1+e^{(\mathcal{E}-\mu)/(k_BT)}}\Big]\mathrm{d}\mathcal{E} \end{aligned} \tag{2.12}$$

which agree with our previous result. It follows from equations (2.10) and (2.10) that the current will respond linearly to the applied bias voltage if the conductance function $G(\mu)$ is independent of energy in the energy range $\mu_D < \mu < \mu_S$.

2.3 Multi-Terminal Conductance

The conductance of multi-terminal scatterer can be calculated by using two-terminal conductances. The total current between terminal i and every other terminal j is a sum of two terminal currents:

$$I_i = \frac{2e}{h} \int \sum_j [T_{ji}(\mathcal{E}) f_i(\mathcal{E}) - T_{ij}(\mathcal{E}) f_j(\mathcal{E})) \mathrm{d}\mathcal{E}. \tag{2.13}$$

As in the two-terminal case, if there is no inelastic scattering, the following relation holds [11]:

$$\sum_j T_{ji}(\mathcal{E}) = \sum_j T_{ij}(\mathcal{E}). \tag{2.14}$$

Thus we can simplify the current formula to read

$$I_i = \frac{2e}{h} \int \sum_j T_{ij}(\mathcal{E}) [f_i(\mathcal{E}) - f_j(\mathcal{E})) \mathrm{d}\mathcal{E}. \tag{2.15}$$

Equation (2.15) is equivalent with

$$I_i = \sum_j G_{ij} [V_i - V_j], \tag{2.16}$$

where G_{ij} is the two-terminal conductance between terminals i and j.

2.4 Scattering Matrix

Let us consider a multi-channel (multi-mode) system in which the input and output leads are identical conductors. Furthermore it is assumed that the number of channels (modes) N is the same in both leads. An incoming wave at mode i in the left lead has a probability $T_{ji} = |t_{ji}|^2$ to be transmitted into mode j in the right lead, and it has a probability $R_{ji} = |r_{ji}|^2$ to be reflected back to the left lead into the mode j. The S-matrix is defined in terms of the transmission and reflection amplitudes, t_{ji} and r_{ji}, as follows

$$S = \begin{bmatrix} r & t' \\ t & r' \end{bmatrix}. \tag{2.17}$$

In equation (2.17) submatrices t, r, t' and r' are $N \times N$ matrices and t' and r' represents the transmission and reflection amplitudes from the right lead into the left and right leads, respectively. If the outgoing amplitudes are represented with $N \times 1$ matrices b and b' and the incoming amplitudes similarly with a and a' on the left and right sides of the scatterer, respectively, the system can be described with equation

$$\begin{bmatrix} b \\ b' \end{bmatrix} = S \cdot \begin{bmatrix} a \\ a' \end{bmatrix} = \begin{bmatrix} r & t' \\ t & r' \end{bmatrix} \begin{bmatrix} a \\ a' \end{bmatrix}. \tag{2.18}$$

Let us denote

$$\tilde{a} = \begin{bmatrix} a \\ a' \end{bmatrix} \quad \text{and} \quad \tilde{b} = \begin{bmatrix} b \\ b' \end{bmatrix}. \tag{2.19}$$

The probability-flux conversation requires that [11]

$$\sum_{m=1}^{2N} |\tilde{a}_m|^2 = \sum_{m=1}^{2N} |\tilde{b}_m|^2 \tag{2.20}$$

which can be written by using adjoint vectors as follows

$$\tilde{a}^\dagger \tilde{a} = \tilde{b}^\dagger \tilde{b}. \tag{2.21}$$

By using equation $\tilde{b} = S\tilde{a}$ we can write

$$\tilde{a}^\dagger \tilde{a} = (S\tilde{a})^\dagger S\tilde{a} = \tilde{a}^\dagger S S^\dagger \tilde{a}, \tag{2.22}$$

from which we see that the S-matrix is unitary i.e.

$$SS^\dagger = S^\dagger S = I. \tag{2.23}$$

Thus we have the following conditions for elements of S

$$\sum_{m=1}^{2N} |s_{mn}|^2 = \sum_{m=1}^{2N} |s_{nm}|^2 = 1. \tag{2.24}$$

Above relation shows that for a given input mode n the sum of the transmission probabilities to all possible output modes m is unity. Equation (2.24) also shows that summing over all possible inputs m for a fixed output n gives as well unity.

Chapter 3

Tunneling Trough Planar Barriers

3.1 Theoretical Model

In the following we consider calculation of transmission coefficient in an arbitrary one-dimensional (1D) potential profile. The aim is to solve the wavefunction on the left side of the barrier (see figure 3.1) when the wavefunction on the right side is known as a boundary condition. The wavefunction on

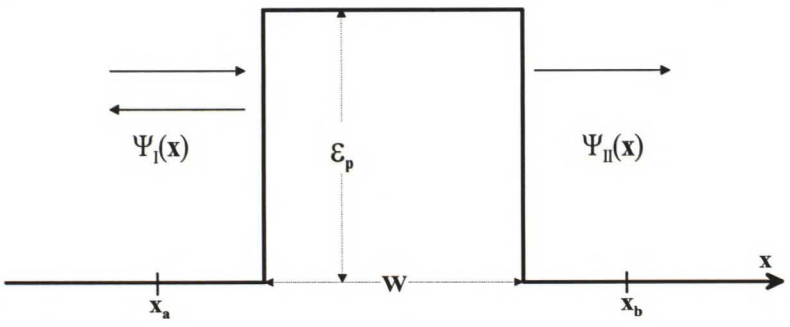

Figure 3.1: 1D rectangular potential barrier.

the l.h.s. of the potential barrier is

$$\Psi_I(x) = Ae^{ikx} + Be^{-ikx}, \tag{3.1}$$

where A and B are the amplitudes of the incoming and reflected waves, respectively. On the r.h.s. of the potential barrier the wavefunction is given by

$$\Psi_{II}(x) = Ce^{ikx}, \tag{3.2}$$

where the amplitude C is set equal to one. Wavefunctions (3.1) and (3.2) fulfill the Schrödinger equation

$$\Big(-\frac{\hbar^2}{2m^*}\frac{\mathrm{d}^2}{\mathrm{d}x^2} + \mathcal{E}_p(x)\Big)\Psi(x) = \mathcal{E}\Psi(x) = \frac{\hbar^2 k^2}{2m^*}\Psi(x), \tag{3.3}$$

where $\mathcal{E}$ is the total energy of particle and $\mathcal{E}_p(x)$ is the potential energy function. In general, the amplitudes A and B in equation (3.1) and the amplitude C in equation (3.2) are complex constants ($C = 1$ was chosen):

$$A = a_r + ia_i \tag{3.4}$$

$$B = b_r + ib_i \tag{3.5}$$

$$C = 1. \tag{3.6}$$

The amplitudes A and B can be solved by using equation (3.2) as a boundary condition for equation (3.1). Let us write equation (3.1) as

$$\Psi_I(x) = Ae^{ikx} + Be^{-ikx} = (a_r + ia_i)e^{ikx} + (b_r + ib_i)e^{-ikx}. \tag{3.7}$$

By taking the real and imaginary parts of equation (3.7), following equations are obtained:

$$\begin{aligned} Re(\Psi_I(x)) &= [a_r\cos(kx) - a_i\sin(kx)] + \\ &\quad + [b_r\cos(kx) + b_i\sin(kx)] \end{aligned} \tag{3.8}$$

$$\begin{aligned} Im(\Psi_I(x)) &= [a_r\sin(kx) + a_i\cos(kx)] + \\ &\quad + [-b_r\sin(kx) + b_i\cos(kx)]. \end{aligned} \tag{3.9}$$

The derivatives of above equations are

$$\begin{aligned} \frac{\mathrm{d}}{\mathrm{d}x}Re(\Psi_I(x)) &= [-ka_r\sin(kx) - ka_i\cos(kx)] + \\ &\quad + [-kb_r\sin(kx) + kb_i\cos(kx)] \end{aligned} \tag{3.10}$$

$$\begin{aligned} \frac{\mathrm{d}}{\mathrm{d}x}Im(\Psi_I(x)) &= [ka_r\cos(kx) - ka_i\sin(kx)] + \\ &\quad + [-kb_r\cos(kx) - kb_i\sin(kx)]. \end{aligned} \tag{3.11}$$

The goal is to calculate the transmission probability which is equal to the square of the ratio of the incoming and transmitted amplitudes:

$$T = \frac{|C|^2}{|A|^2} = \frac{1}{\left(\sqrt{a_r^2 + a_i^2}\right)^2} = \frac{1}{a_r^2 + a_i^2} \tag{3.12}$$

3.2 Calculations

Numerical solutions for the real and imaginary parts of $\Psi_I(x)$ and their derivatives are obtained by writing the Schrödinger equation (3.3) as a system of two first order coupled differential equations which are solved by using finite difference methods. Furthermore the equation (3.2) is used as boundary condition at $x_0 = x_b$ (see Fig. 3.1) and the real and imaginary parts of the solution are calculated separately. The system of two first order equations is

$$\begin{cases} \Psi'(x) &= \Phi(x) \\ \Phi'(x) &= \frac{2m^*}{\hbar^2}[\mathcal{E}_p(x) - \mathcal{E}]\Psi(x). \end{cases} \tag{3.13}$$

The first step is calculated with the forward Euler method [12, 13]:

$$y_1 = y_0 + \delta f(x_0, y_0). \tag{3.14}$$

And the other steps ($n \geq 2$) are calculated with the midpoint method [12, 13]:

$$y_n = y_{n-2} + 2\delta f(x_{n-1}, y_{n-1}). \tag{3.15}$$

In the above equations δ ($=x_{n+1} - x_n$) is the step size and $f(x_n, y_n)$ corresponds to the r.h.s of equations (3.13).

The real and imaginary parts of $\Psi_I(x)$ and their derivatives are denoted by

$$\begin{cases} R(x) &= Re(\Psi_I(x)) \\ I(x) &= Im(\Psi_I(x)) \\ DR(x) &= \mathrm{d}R(x)/\mathrm{d}x \\ DI(x) &= \mathrm{d}I(x)/\mathrm{d}x \end{cases} . \tag{3.16}$$

By setting equation (3.1) equal to numerical solution at some point $x = x_a$ which is located on the l.h.s. of the barrier (see Fig. 3.1), A and B can be solved. Thus the following system of equations is obtained:

$$\begin{cases} R(x_a) &= (a_r + b_r)\cos(kx_a) + (-a_i + b_i)\sin(kx_a) \\ I(x_a) &= (a_r - b_r)\sin(kx_a) + (a_i + b_i)\cos(kx_a) \\ DR(x_a) &= k(-a_r - b_r)\sin(kx_a) + k(-a_i + b_i)\cos(kx_a) \\ DI(x_a) &= k(a_r - b_r)\cos(kx_a) + k(-a_i - b_i)\sin(kx_a) \end{cases} . \tag{3.17}$$

Now we can solve a_r, b_r, a_i and b_i from above system of equations. We get

$$\begin{cases} kR(x_a) + DI(x_a) &= 2ka_r\cos(kx_a) - 2ka_i\sin(kx_a) \\ kI(x_a) - DR(x_a) &= 2ka_r\sin(kx_a) + 2ka_i\cos(kx_a) \\ kR(x_a) - DI(x_a) &= 2kb_r\cos(kx_a) + 2kb_i\sin(kx_a) \\ kI(x_a) + DR(x_a) &= -2kb_r\sin(kx_a) + 2kb_i\cos(kx_a) \end{cases} \tag{3.18}$$

$\Longleftrightarrow$

$$\begin{cases} \frac{kR(x_a)+DI(x_a)}{\sin(kx_a)} + \frac{kI(x_a)-DR(x_a)}{\cos(kx_a)} &= 2ka_r[\cot(kx_a) + \tan(kx_a)] \\ \frac{kR(x_a)+DI(x_a)}{\cos(kx_a)} - \frac{kI(x_a)-DR(x_a)}{\sin(kx_a)} &= -2ka_i[\cot(kx_a) + \tan(kx_a)] \\ \frac{kR(x_a)-DI(x_a)}{\sin(kx_a)} - \frac{kI(x_a)+DR(x_a)}{\cos(kx_a)} &= 2kb_r[\cot(kx_a) + \tan(kx_a)] \\ \frac{kR(x_a)-DI(x_a)}{\cos(kx_a)} + \frac{kI(x_a)+DR(x_a)}{\sin(kx_a)} &= 2kb_i[\cot(kx_a) + \tan(kx_a)] \end{cases} \tag{3.19}$$

$\Longleftrightarrow$

$$\begin{cases} a_r &= \frac{1}{2k}\left(\frac{kR(x_a)+DI(x_a)}{\sin(kx_a)} + \frac{kI(x_a)-DR(x_a)}{\cos(kx_a)}\right)\frac{1}{\cot(kx_a)+\tan(kx_a)} \\ a_i &= -\frac{1}{2k}\left(\frac{kR(x_a)+DI(x_a)}{\cos(kx_a)} - \frac{kI(x_a)-DR(x_a)}{\sin(kx_a)}\right)\frac{1}{\cot(kx_a)+\tan(kx_a)} \\ b_r &= \frac{1}{2k}\left(\frac{kR(x_a)-DI(x_a)}{\sin(kx_a)} - \frac{kI(x_a)+DR(x_a)}{\cos(kx_a)}\right)\frac{1}{\cot(kx_a)+\tan(kx_a)} \\ b_i &= \frac{1}{2k}\left(\frac{kR(x_a)-DI(x_a)}{\cos(kx_a)} + \frac{kI(x_a)+DR(x_a)}{\sin(kx_a)}\right)\frac{1}{\cot(kx_a)+\tan(kx_a)} \end{cases} . \tag{3.20}$$

By substituting a_i and a_r into equation (3.12) we get the transmission coefficient.

3.2.1 Single Potential Barrier

A comparison of numerically and analytically calculated transmission probabilities is represented in figure 3.2. The analytic solutions for the transmission

coefficients through the single rectangular potential barrier are [14]:

$$T_{\mathcal{E}>\mathcal{E}_p} = \frac{1}{1+\frac{1}{4}\frac{\mathcal{E}_p^2}{\mathcal{E}(\mathcal{E}-\mathcal{E}_p)}\sin^2\left(\sqrt{\frac{2m(\mathcal{E}-\mathcal{E}_p)}{\hbar^2}}a\right)} \tag{3.21}$$

$$T_{\mathcal{E}<\mathcal{E}_p} = \frac{1}{1+\frac{1}{4}\frac{\mathcal{E}_p^2}{\mathcal{E}(\mathcal{E}_p-\mathcal{E})}\sinh^2\left(\sqrt{\frac{2m(\mathcal{E}_p-\mathcal{E})}{\hbar^2}}a\right)}, \tag{3.22}$$

where a and $\mathcal{E}_p$ are the width and height of the potential barrier, respectively. The numerical and analytical solutions agree within the numerical accuracy of the calculations.

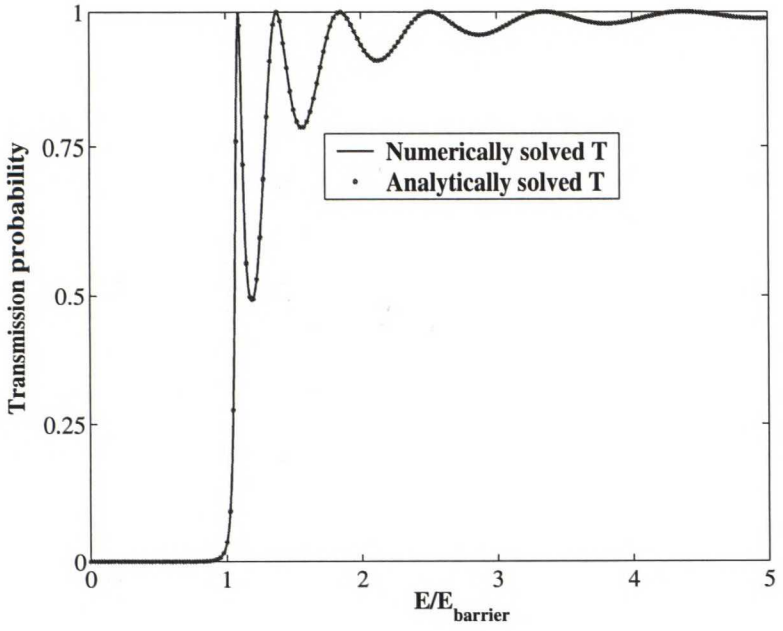

Figure 3.2: Transmission probability for a single potential barrier. The width of the barrier is 2 nm and the the potential energy of the barrier is 1 eV. For the electron mass we used the rest mass m_0.

3.2.2 Double Barrier

The 1D double potential barrier structure is also known as a resonant tunneling diode. Figure 3.2 represents the transmission in a double barrier struc-

ture. Note the prominent resonant tunneling effects.

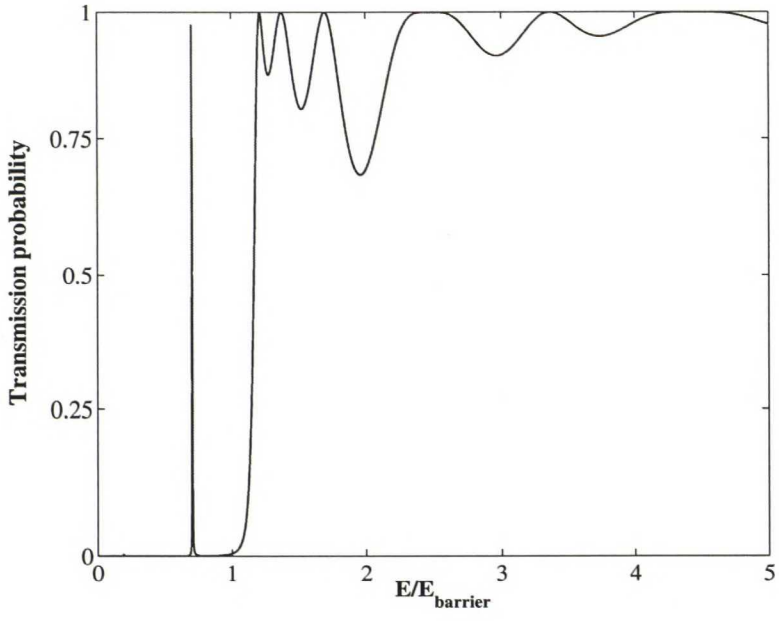

Figure 3.3: Transmission probability for double potential barrier. Two 1 eV high and 1 nm wide barriers are separated with 1 nm. The used mass was the electron rest mass

Chapter 4

Mode Matching Method

4.1 Introduction

First the mode matching method [15, 16, 17] is formulated for systems where the Schrödinger equation is two dimensional and subsequently the method is generalized for conducting channels where electron wavefunctions depend on all three spatial coordinates.

Structures where the electrons are confined in 2D are treated in section 4.2. This corresponds to situation e.g. in MOSFETs. In quantum wires (QWR) and quantum point contacts (QPC) the movement of electrons is confined in 1D. This kind of conducting channels are treated in section 4.3.

4.2 Mode Matching Method in Two-Dimensional Structure

4.2.1 Technique for Single Junction

In a uniform quantum waveguide the Schrödinger equation can be separated to transversal (x-coordinate) and propagating (z-coordinate) parts and its

solution is (see figure 4.1) given by

$$\psi_n = \phi_n(x)(A_n e^{ik(n)z} + B_n e^{-ik(n)z}). \tag{4.1}$$

To analyze a nonuniform waveguide configuration with the mode matching method, the structure must be divided into uniform waveguide sections. Then each section can be characterized by a generalized scattering matrix (GSM) whose elements are the modal scattering parameters including those for evanescent modes. The GSM of the nonuniform waveguide structure is obtained by combining the GSMs of the uniform sections.

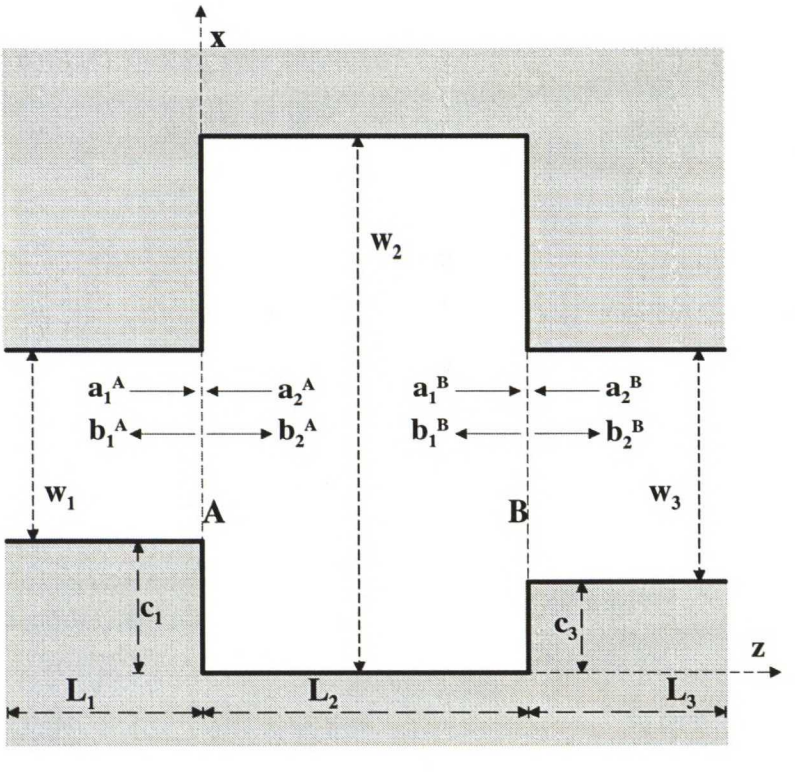

Figure 4.1: 2D rectangular potential stub. Potential energy is infinite in the shaded areas and zero elsewhere.

First we derive the GSMs for a uniform waveguide and for a single junction and in the next section for the whole conducting potential structure. In general the wavefunctions on different sides of the junction are (see Figure

4.1)

$$\psi_1 = \phi_1^T(P_1 a_1 + P_1^{-1} b_1) \text{ and} \tag{4.2}$$

$$\psi_2 = \phi_2^T(P_2 a_2 + P_2^{-1} b_2), \tag{4.3}$$

where $a_{1,2}$ and $b_{1,2}$ are column vectors whose elements are the amplitudes of the corresponding modes and $P_{1,2}$ are diagonal matrices defined as

$$P_{1,2}(n,n) = e^{ik_{1,2}(n)z}. \tag{4.4}$$

The elements of the column vectors $\phi_{1,2}$ are orthonormal eigenfunctions which are defined as

$$\phi_{1,2}(n) = \sqrt{\frac{2}{w_{1,2}}} \sin(\frac{n\pi}{w_{1,2}} x), \tag{4.5}$$

where $w_{1,2}$ are the widths of the channel in the x-direction (i.e. perpendicular to propagation direction) on different sides of the junction. The wavevectors in equation (4.4) are defined as

$$k_{1,2}(n) = \sqrt{\frac{2m^*}{\hbar^2}(\mathcal{E} - V) - (\frac{n\pi}{w_{1,2}})^2}, \tag{4.6}$$

where m^* is the effective mass (see section 1.3), V is the potential energy and $\mathcal{E}$ is the total energy of particle. The continuity condition for the wavefunctions and its normal derivative at the junction gives us the following two equations for junction A in Fig. 4.1 when the junction is located at $z = 0$:

$$\phi_2^T(a_2 + b_2) = \begin{cases} \phi_1^T(a_1 + b_1), & c_1 \le x \le c_1 + w_1 \\ 0, & \text{otherwise} \end{cases} \tag{4.7}$$

$$\phi_1^T K_1(a_1 - b_1) = \phi_2^T K_2(b_2 - a_2), \quad c_1 \le x \le c_1 + w_1, \tag{4.8}$$

where $K_{1,2}$ are diagonal matrices whose elements are defined in equation (4.6).

Next we construct the GSM for a single junction A by multiplying equation (4.7) by $\phi_2(m)$ and equation (4.8) by $\phi_1(m)$, by integrating with regard to x and by using the orthonormality of the eigenfunctions ϕ_1 and ϕ_2. Thus we

get

$$H_1(a_1 + b_1) = a_2 + b_2 \tag{4.9}$$

$$a_1 - b_1 = H_2(a_2 - b_2), \tag{4.10}$$

where

$$H_1 = C \tag{4.11}$$

and

$$H_2 = -K_1^{-1} C^T K_2. \tag{4.12}$$

Above the C matrix characterizes the mode coupling due the step discontinuity. It is defined in terms of the overlap integrals as follows:

$$C_{mn} = \int_c^w \phi_1(n)\phi_2(m)\mathrm{d}x. \tag{4.13}$$

Now the generalized scattering matrix for a single junction is obtained from equations (4.9) and (4.10). The GSM for the step discontinuity fulfills

$$\begin{bmatrix} b_1^A \\ b_2^A \end{bmatrix} = \begin{bmatrix} S_{11}^A & S_{12}^A \\ S_{21}^A & S_{22}^A \end{bmatrix} \begin{bmatrix} a_1^A \\ a_2^A \end{bmatrix}, \tag{4.14}$$

where the submatrices of GSM for the junction A are

$$S_{11}^A = (I - H_2H_1)^{-1}(I + H_2H_1), \tag{4.15}$$

$$S_{12}^A = -2(I - H_2H_1)^{-1}H_2, \tag{4.16}$$

$$S_{21}^A = H_1(I + S_{11}), \tag{4.17}$$

$$S_{22}^A = H_1S_{12} - I. \tag{4.18}$$

Similarly we obtain the generalized scattering matrix for the junction B in Fig. 4.1. The continuity conditions for the junction B (the junction B is located at $z = 0$) lead to equations

$$\phi_1^T(a_1 + b_1) = \begin{cases} \phi_2^T(a_2 + b_2), & c_3 \le x \le c_3 + w_3 \\ 0, & \text{otherwise} \end{cases} \tag{4.19}$$

$$\phi_1^T K_1(a_1 - b_1) = \phi_2^T K_2(b_2 - a_2), \quad c_3 \le x \le c_3 + w_3. \tag{4.20}$$

Next equation (4.19) is multiplied by $\phi_1(m)$ and equation (4.20) is multiplied by $\phi_2(m)$, and both equations are integrated with regard to x. As a result we obtain

$$a_1 + b_1 = H_1(a_2 + b_2) \tag{4.21}$$

$$H_2(a_1 - b_1) = b_2 - a_2, \tag{4.22}$$

where

$$H_1 = C^T \tag{4.23}$$

and

$$H_2 = K_2^{-1} C K_1. \tag{4.24}$$

The matrix equation for the junction B is given in analogy to equation (4.14) by

$$\begin{bmatrix} b_1^B \\ b_2^B \end{bmatrix} = \begin{bmatrix} S_{11}^B & S_{12}^B \\ S_{21}^B & S_{22}^B \end{bmatrix} \begin{bmatrix} a_1^B \\ a_2^B \end{bmatrix} \tag{4.25}$$

with submatrices

$$S_{11}^B = (I + H_1 H_2)^{-1}(-I + H_1 H_2), \tag{4.26}$$

$$S_{12}^B = 2(I + H_1 H_2)^{-1} H_1, \tag{4.27}$$

$$S_{21}^B = H_2(I - S_{11}) \tag{4.28}$$

$$S_{22}^B = I - H_2 S_{12} \tag{4.29}$$

Thus we see that the equations depend on which side of the junction is narrower. Therefore from here on we will always denote the narrower side of the junction as the "side 1" and use equations (4.15)-(4.18).

The GSM for a uniform waveguide section of length L_2 (the middle section in figure 4.1) is a special case and can be expressed as follows

$$\begin{bmatrix} S_{11} & S_{12} \\ S_{21} & S_{22} \end{bmatrix} = \begin{bmatrix} 0 & P \\ P & 0 \end{bmatrix}, \tag{4.30}$$

where 0 is the null matrix and P is a diagonal matrix given by

$$P(n, n) = e^{ik(n)L_2}. \tag{4.31}$$

This can be verified with the following reasoning: Let us locate the junction A at $z = 0$. Then the junction B is located at $z = L_2$ (see figure 4.1). The wavefunction of the middle section on the edge A is $\phi^T(b_2^A + a_2^A)$ and on the edge B it is $\phi^T(P(z = L_2)a_1^B + P^{-1}(z = L_2)b_1^B)$. Thus $b_2^A = P(z = L_2)a_1^B$ and $b_1^B = P(z = L_2)a_2^A$ and equation (4.30) follows.

4.2.2 Technique for 2D Potential Stub

The total number of modes on each side of the junction A (N_1^A and N_2^A) may, in general, be different depending on how many evanescent modes in each junction is taken into account to obtain the required accuracy. We use $K \leq \min\{N_1^A, N_2^A\}$ modes in the calculations. Thus the mode vector a_1^A, which represents the incoming amplitudes on the left side of the junction A, is partitioned into the mode vector a_a^A with elements a_i^A $(i = 1, \ldots, K)$ and into the mode vector a_b^A with elements a_i^A $(i = K+1, \ldots, N_1^A)$. Vectors a_2^A, b_1^A and b_2^A are partitioned in a similar manner (see figure 4.1).

The partitioned GSM of the junction A can be expressed as

$$\begin{aligned}\begin{bmatrix} b_1^A \\ b_2^A \end{bmatrix} &= \begin{bmatrix} b_a^A \\ b_b^A \\ b_c^A \\ b_d^A \end{bmatrix} = \begin{bmatrix} S_{aa}^A & S_{ab}^A & S_{ac}^A & S_{ad}^A \\ S_{ba}^A & S_{bb}^A & S_{bc}^A & S_{bd}^A \\ S_{ca}^A & S_{cb}^A & S_{cc}^A & S_{cd}^A \\ S_{da}^A & S_{db}^A & S_{dc}^A & S_{dd}^A \end{bmatrix} \begin{bmatrix} a_a^A \\ a_b^A \\ a_c^A \\ a_d^A \end{bmatrix} \\ &= \begin{bmatrix} S_{11}^A & S_{12}^A \\ S_{21}^A & S_{22}^A \end{bmatrix} \begin{bmatrix} a_1^A \\ a_2^A \end{bmatrix}. \end{aligned} \tag{4.32}$$

The corresponding partitioned GSM for the junction B is

$$\begin{aligned}\begin{bmatrix} b_1^B \\ b_2^B \end{bmatrix} &= \begin{bmatrix} b_a^B \\ b_b^B \\ b_c^B \\ b_d^B \end{bmatrix} = \begin{bmatrix} S_{aa}^B & S_{ab}^B & S_{ac}^B & S_{ad}^B \\ S_{ba}^B & S_{bb}^B & S_{bc}^B & S_{bd}^B \\ S_{ca}^B & S_{cb}^B & S_{cc}^B & S_{cd}^B \\ S_{da}^B & S_{db}^B & S_{dc}^B & S_{dd}^B \end{bmatrix} \begin{bmatrix} a_a^B \\ a_b^B \\ a_c^B \\ a_d^B \end{bmatrix} \\ &= \begin{bmatrix} S_{11}^B & S_{12}^B \\ S_{21}^B & S_{22}^B \end{bmatrix} \begin{bmatrix} a_1^B \\ a_2^B \end{bmatrix}. \end{aligned} \tag{4.33}$$

Now by using equation (4.32) for the junction A, equation (4.30) for the uniform waveguide and equation (4.33) for the junction B, we get the GSM for the whole structure. The matrix equation can be written as

$$\begin{bmatrix} b_1 \\ b_2 \end{bmatrix} = \begin{bmatrix} b_a^A \\ b_b^A \\ b_a^B \\ b_b^B \end{bmatrix} = \begin{bmatrix} S_{11} & S_{12} \\ S_{21} & S_{22} \end{bmatrix} \begin{bmatrix} a_a^A \\ a_b^A \\ a_a^B \\ a_b^B \end{bmatrix} = \begin{bmatrix} S_{11} & S_{12} \\ S_{21} & S_{22} \end{bmatrix} \begin{bmatrix} a_1 \\ a_2 \end{bmatrix}, \quad (4.34)$$

where the submatrices of the GSM are given by [15]:

$$S_{11} = \begin{bmatrix} S_{aa}^A & S_{ab}^A \\ S_{ba}^A & S_{bb}^A \end{bmatrix} + \begin{bmatrix} S_{ac}^A P(I - S_{cc}^B P S_{cc}^A P)^{-1} S_{cc}^B P \begin{bmatrix} S_{ca}^A & S_{cb}^A \end{bmatrix} \\ S_{bc}^A P(I - S_{cc}^B P S_{cc}^A P)^{-1} S_{cc}^B P \begin{bmatrix} S_{ca}^A & S_{cb}^A \end{bmatrix} \end{bmatrix} \quad (4.35)$$

$$S_{12} = \begin{bmatrix} S_{ac}^A P(I - S_{cc}^B P S_{cc}^A P)^{-1} \begin{bmatrix} S_{ca}^B & S_{cb}^B \end{bmatrix} \\ S_{bc}^A P(I - S_{cc}^B P S_{cc}^A P)^{-1} \begin{bmatrix} S_{ca}^B & S_{cb}^B \end{bmatrix} \end{bmatrix} \quad (4.36)$$

$$S_{21} = \begin{bmatrix} S_{ac}^B P(I - S_{cc}^A P S_{cc}^B P)^{-1} \begin{bmatrix} S_{ca}^A & S_{cb}^A \end{bmatrix} \\ S_{bc}^B P(I - S_{cc}^A P S_{cc}^B P)^{-1} \begin{bmatrix} S_{ca}^A & S_{cb}^A \end{bmatrix} \end{bmatrix} \quad (4.37)$$

$$S_{22} = \begin{bmatrix} S_{aa}^B & S_{ab}^B \\ S_{ba}^B & S_{bb}^B \end{bmatrix} + \begin{bmatrix} S_{ac}^B P(I - S_{cc}^A P S_{cc}^B P)^{-1} S_{cc}^A P \begin{bmatrix} S_{ca}^B & S_{cb}^B \end{bmatrix} \\ S_{bc}^B P(I - S_{cc}^A P S_{cc}^B P)^{-1} S_{cc}^A P \begin{bmatrix} S_{ca}^B & S_{cb}^B \end{bmatrix} \end{bmatrix} \quad (4.38)$$

The transmission coefficient can now be calculated by using equation (4.37) and equation (4.6) as follows

$$T = \sum_n \frac{\sum_m S_{21}(m,n) S_{21}^*(m,n)(k_2^B(m) + k_2^{B*}(m))}{k_1^A(n) + k_1^{A*}(n)}. \quad (4.39)$$

Previous derivation is valid for cases like the one seen in figure 4.1, but if the l.h.s. of the junction A is wider than the r.h.s. the GSM for the junction A must be reorganized. Correspondingly, if the l.h.s. of the junction B is narrower than the r.h.s., the GSM for the junction B must be reorganized. The need to reorganize the matrix equations (4.32) and (4.33) is that they were established by considering the structure as in figure 4.1. However we always denote the mode vectors of the narrower side of the junction as a_1 and b_1 and furthermore we want to represent the outcoming mode amplitudes b_1

and b_2 of the scatterer as function of the incoming mode amplitudes a_1 and a_2. Thus, if for example $w_1 > w_2$ for the junction A (see figure 4.1) the matrix equations must be written as

$$\begin{bmatrix} b_1' \\ b_2' \end{bmatrix} = \begin{bmatrix} b_2 \\ b_1 \end{bmatrix} = \begin{bmatrix} S_{22} & S_{21} \\ S_{12} & S_{11} \end{bmatrix} \begin{bmatrix} a_2 \\ a_1 \end{bmatrix} = \begin{bmatrix} S_{22} & S_{21} \\ S_{12} & S_{11} \end{bmatrix} \begin{bmatrix} a_1' \\ a_2' \end{bmatrix}. \quad (4.40)$$

From equation (4.40) it follows that the reorganized matrices are

$$GSM_{ro}^{A} = \begin{bmatrix} S_{22}^{A} & S_{21}^{A} \\ S_{12}^{A} & S_{11}^{A} \end{bmatrix} \quad (4.41)$$

and

$$GSM_{ro}^{B} = \begin{bmatrix} S_{22}^{B} & S_{21}^{B} \\ S_{12}^{B} & S_{11}^{B} \end{bmatrix} \quad (4.42)$$

where the submatrices S_{11}, S_{12}, S_{21} and S_{22} were defined in equations (4.15)-(4.18).

4.2.3 2D Potential Structure

In the case of arbitrary number of junctions the mode matching method is used recursively: the method of section 4.2.2 is used for the first two junctions, then step by step the previously computed GSM and the GSM for the next junction are combined by using methods described in the preceding section. This procedure is continued until GSM for the whole structure is computed. It has to be emphasized that the submatrices in equations (4.15)-(4.18) are derived for the waveguide depicted in figure 4.1. When needed the generalized scattering matrices must be reorganized as mentioned at the end of section 4.2.2.

4.3 Mode Matching Method in Three-Dimensional Structure

4.3.1 Transversal States

Now the solution for Schrödinger equation depends on all three spatial coordinates

$$\psi_n(x,y,z) = \phi_n(x,y)(A_n e^{ik(n)z} + B_n e^{-ik(n)z}). \tag{4.43}$$

The method of calculations of the 3D case is the same as in the 2D case except that the transversal states are now functions of two coordinates. In arbitrary case $\phi_n(x,y)$ in equation (4.43) can not be solved analytically. We use finite difference method for solving $\phi_n(x,y)$.

For finding $\phi_n(x,y)$ in equation (4.43), we must solve 2D Schrödinger equation

$$\Big(-\frac{\hbar^2}{2m^*}\nabla^2 + V(x,y)\Big)\phi_n(x,y) = \mathcal{E}_n\phi_n(x,y). \tag{4.44}$$

This is done by using the five point finite difference scheme for ∇^2 in (4.44) i.e. by using

$$\nabla^2\phi_{i,j} = \frac{\phi_{i,j+1} - 2\phi_{i,j} + \phi_{i,j-1}}{\delta^2} + \frac{\phi_{i+1,j} - 2\phi_{i,j} + \phi_{i-1,j}}{\delta^2}, \tag{4.45}$$

where δ is the step length and j and i are the coordinate indexes i.e. the discretized coordinates. Solving equation (4.44) as a boundary value problem (at the boundaries $\phi \equiv 0$) leads us to an eigenvalue problem

$$\Delta\phi_n = \mathcal{E}_n\phi_n, \tag{4.46}$$

where

$$\phi_n = \begin{bmatrix} \phi^n_{1,1} \\ \phi^n_{1,2} \\ \vdots \\ \phi^n_{i_{max},j_{max}} \end{bmatrix} \tag{4.47}$$

and

$$\Delta = \begin{bmatrix} \frac{2\hbar^2}{m\delta^2} + V_{1,1} & -\frac{\hbar^2}{2m\delta^2} & & \cdots & -\frac{\hbar^2}{2m\delta^2} & \\ -\frac{\hbar^2}{2m\delta^2} & \frac{2\hbar^2}{m\delta^2} + V_{1,2} & -\frac{\hbar^2}{2m\delta^2} & & & \ddots \\ & -\frac{\hbar^2}{2m\delta^2} & \frac{2\hbar^2}{m\delta^2} + V_{1,3} & -\frac{\hbar^2}{2m\delta^2} & & \\ & & \ddots & \ddots & \ddots & \\ \vdots & & & & & \\ -\frac{\hbar^2}{2m\delta^2} & & & & & \\ & \ddots & & & & \end{bmatrix}. \quad (4.48)$$

In equation (4.48) δ is the step size and $V_{i,j}$ is the potential energy at point (i, j).

4.3.2 Generalized Scattering Matrix

The GSM is build up with the same algorithm as in the 2D case. First we form GSMs for the first two single junctions and combine those to one GSM. Then step by step the GSM for the next single junction is formed and it is combined with the existing GSM. This is continued until the GSM for the whole structure is formed. Overlap-integrals must now be calculated over the whole area where the transversal states at opposite sides of junction overlap. Thus the integral is two dimensional:

$$C_{mn} = \int_{\Omega} \phi_1(n, x, y)\phi_2(m, x, y)\mathrm{d}\Omega, \quad (4.49)$$

where Ω is a set of such points (x, y), where the transversal state n at the l.h.s. of the junction and the transversal state m at the r.h.s. of the junctions overlap each other. Also the equation for the wavevector is now chanced into form

$$k(n) = \sqrt{\frac{2m^*}{\hbar}(\mathcal{E} - V - \mathcal{E}_n)}, \quad (4.50)$$

where $\mathcal{E}$ is the total energy of the particle, V is the potential energy and $\mathcal{E}_n$ is the energy of the nth transversal state.

4.4 Results of Calculations

4.4.1 T-Stub

Figure 4.2 represents the transmission probability in the T-stub as a function of energy. The dimensions in the T-stub corresponding to the figure 4.1 are $c_1 = c_3 = 0\ nm$, $w_1 = \frac{1}{2}w_2 = w_3 = 10\ nm$ and $L_1 = L_2 = L_3 = 10\ nm$. For the effective mass we used a value $m^* = 0.05m_0$.

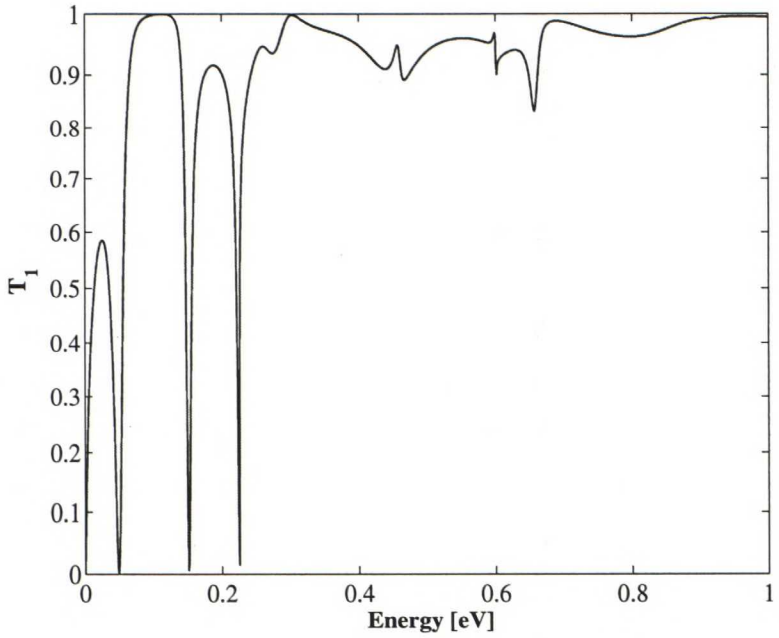

Figure 4.2: The total transmission probability from mode 1 (ground state) to any transverse mode on the other side of the scatterer. The waveguide is 10 nm wide and the size of stub is 10 nm × 10 nm. The zero of the energy axis corresponds to ground state energy of the lead: $\mathcal{E}_1 = \hbar^2\pi^2/(2m^*w_1^2) \approx 75\ meV$, $m^* = 0.05m_0$. The present results agree very well with those obtained in reference [18].

4.4.2 Resonance

Let us consider a two-dimensional potential structure where a constriction is between 200 nm wide leads. The length and width of the constriction are altered between 0 and 200 nm. In figure 4.3 the conductance (the relation between conductance and transmission coefficient was derived in chapter 2.2) is plotted as function of the width and length of the constriction. Clear

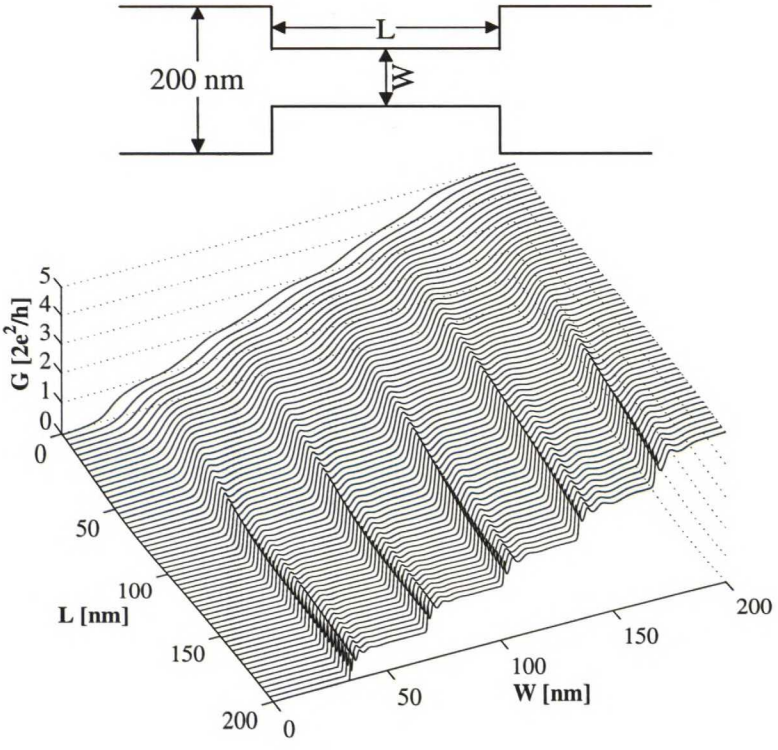

Figure 4.3: Above: The constriction is located between 200 nm wide leads. Below: The conductance of the constriction as a function of the width (W) and length (L) of the constriction at $T = 0\ K$. The energy of particles is $\mathcal{E} = 5\ meV$ and the effective mass is $m^* = 0.067m_0$.

resonance effects are seen with long constriction, but those totally vanish when the constriction become shorter.

4.4.3 Quantum Point Contact

Our goal was to calculate the conductance of silicon quantum point contact (QPC) shown in figure 4.4. Because the channel is in the [110] direction we rotate the coordinate system so that z is in the [001] direction, y is along the channel, and x is perpendicular to the wire (i.e. x-axis was rotated in the (001) plane by angle of θ from [100] towards [010]). Therefore the effective masses of silicon was calculated by using $\theta = \pi/4$ (see section 1.3.4). The

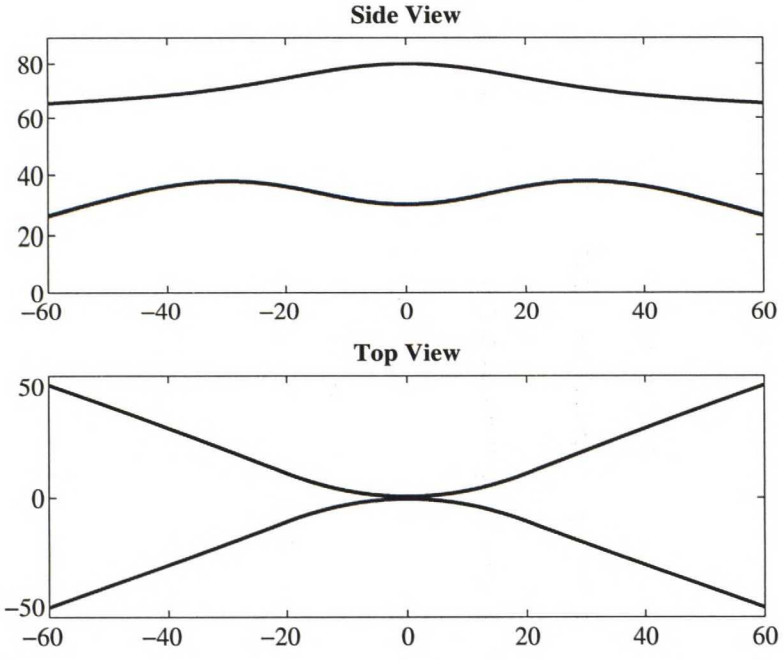

Figure 4.4: Structure of the modeled QPC. Dimensions are in nanometers.

calculations were performed by using the 3D mode matching method, which was introduced in section 4.3. The calculated conductance at zero temperature is given in figure 4.5 and at 1.5 K in figure 4.6. Clear conductance steps are seen at $T = 0\ K$ but at $T = 1.5\ K$ the steps are smoother.

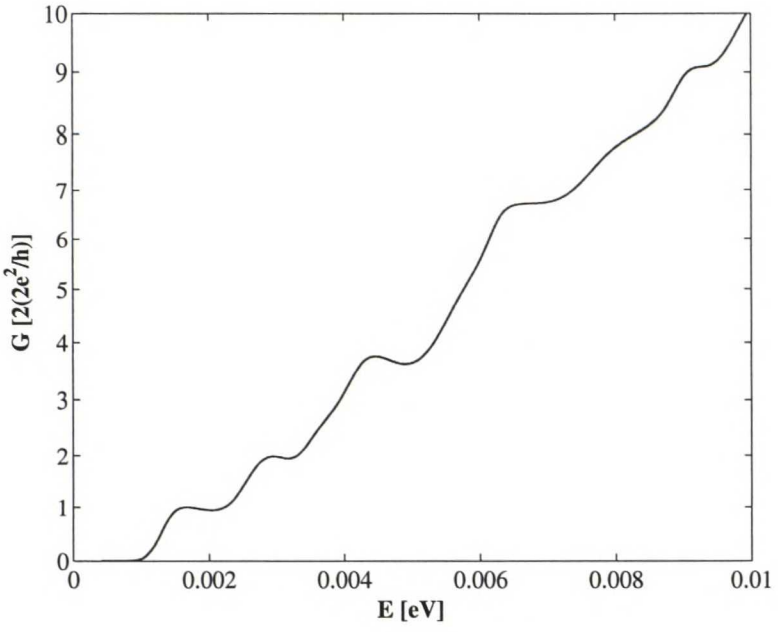

Figure 4.5: Calculated conductance of the QPC in fig. 4.4 at $T = 0$K.

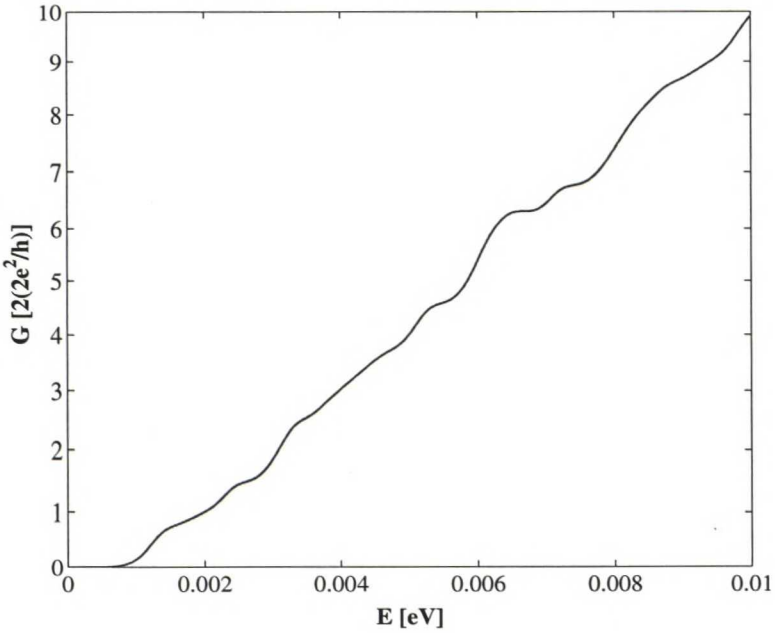

Figure 4.6: Calculated conductance of the QPC in fig. 4.4 at $T = 1.5$K.

Chapter 5

Lattice Green's Function Method

5.1 Introduction

The Green's function method [13, 17, 19] offers an alternative method for solving inhomogeneous linear partial differential equations with homogeneous or inhomogeneous boundary conditions.

5.2 Single-Particle Green's Function

The time-independent Schrödinger equation can be written as

$$\mathcal{H}\Psi = \mathcal{E}\Psi \tag{5.1}$$

or equivalently

$$[\mathcal{E}\mathcal{I} - \mathcal{H}]\Psi = 0, \tag{5.2}$$

where $\mathcal{H}$ is the single-particle Hamiltonian and $\mathcal{E}$ is the total energy of the particle. The Hamiltonian operator $\mathcal{H}$ is a Hermitian operator and it obeys eigenvalue equation

$$\mathcal{H}|\Phi_n\rangle = \mathcal{E}_n|\Phi_n\rangle, \tag{5.3}$$

where all eigenvalues $\mathcal{E}_n$ are real and eigenfunctions $|\Phi_n\rangle$ (see appendix A for more details about the "bracket" notation) form a complete set of states:

$$\begin{cases} \sum_n' |\Phi_n\rangle\langle\Phi_n| = \mathcal{I} & \text{(completeness)} \\ \langle\Phi_n|\Phi_m\rangle = \delta_{nm} & \text{(orthonormality).} \end{cases} \tag{5.4}$$

In the completeness relation $\sum_n'$ indicates a sum over the discrete eigenstates as well as an integration over the continuous part of the spectrum. $\mathcal{I}$ denotes the identity operator.

The Green's function operator corresponding to equation (5.2) is defined by

$$[\mathcal{E}\mathcal{I} - \mathcal{H}]\mathbf{G}(\mathcal{E}) = \mathcal{I}, \tag{5.5}$$

where the Green's function operator $\mathbf{G}(\mathcal{E})$ fulfills the same boundary conditions as the wave-function Ψ in equation (5.2) and it can be written as

$$\mathbf{G}(\mathcal{E}) = [\mathcal{E}\mathcal{I} - \mathcal{H}]^{-1}. \tag{5.6}$$

Because $\mathbf{G}(\mathcal{E})$ has singularities at energies $\mathcal{E} = \mathcal{E}_n$, we must define

$$\mathbf{G}^{\pm}(\mathcal{E}) = \lim_{\eta \to 0^+} \mathbf{G}(\mathcal{E} \pm i\eta). \tag{5.7}$$

If we furthermore assume that η is infinitesimal, we can write

$$\mathbf{G}^{\pm}(\mathcal{E}) = [(\mathcal{E} \pm i\eta)\mathcal{I} - \mathcal{H}]^{-1}. \tag{5.8}$$

Next we want to express the Green's function by using the eigenvalues and the eigenstates of $\mathcal{H}$. The spectral representation of the Green's function is

$$\mathbf{G}^{\pm}(\mathcal{E}) = [(\mathcal{E} \pm i\eta)\mathcal{I} - \mathcal{H}]^{-1} = \sum_n{}' \frac{|\Phi_n\rangle\langle\Phi_n|}{\mathcal{E} - \mathcal{E}_n \pm i\eta}. \tag{5.9}$$

Equation (5.9) can be verified by using $\mathcal{H} = \sum_n' \mathcal{E}_n |\Phi_n\rangle\langle\Phi_n|$, $\mathcal{I} = \sum_n' |\Phi_n\rangle\langle\Phi_n|$ and the following reasoning:

$$(\mathcal{E}\mathcal{I} - \mathcal{H})\mathbf{G}(\mathcal{E}) = \Big(\sum_n{}'(\mathcal{E} - \mathcal{E}_n)|\Phi_n\rangle\langle\Phi_n|\Big)\Big(\sum_m{}' \frac{|\Phi_m\rangle\langle\Phi_m|}{\mathcal{E} - \mathcal{E}_m}\Big)$$

$$
\begin{aligned}
&= \sum_{n}{}' \sum_{m}{}' (\mathcal{E} - \mathcal{E}_n)|\Phi_n\rangle\langle\Phi_n| \frac{|\Phi_m\rangle\langle\Phi_m|}{\mathcal{E} - \mathcal{E}_m} \\
&= \sum_{n}{}' \sum_{m}{}' |\Phi_n\rangle\delta_{nm}\langle\Phi_m| \frac{\mathcal{E} - \mathcal{E}_n}{\mathcal{E} - \mathcal{E}_m} \\
&= \sum_{n}{}' |\Phi_n\rangle\langle\Phi_n| = \mathcal{I}. \qquad (5.10)
\end{aligned}
$$

From equation (5.10) one obtains equation (5.9) by substitution $\mathcal{E} := \mathcal{E} \pm i\eta$. The $+$ and $-$ signs at $\mathbf{G}^{\pm}(\mathcal{E})$ correspond to different boundary conditions and are called retarded and advanced Green's functions [17, 11], respectively.

5.3 Tight-Binding Model

The tight binding model is a numerical model which can be used to find the eigenfunctions of one electron Schrödinger equation (5.2). The Hamiltonian of an electron is discretized by using the complete set of states $|\mathbf{r}\rangle$ formed by the lattice site vectors $\mathbf{r}$. This is called as the tight-binding Hamiltonian and it can be written as

$$\mathcal{H} = \sum_{\mathbf{r}} |\mathbf{r}\rangle\mathcal{E}_{\mathbf{r}}\langle\mathbf{r}| + \sum_{\mathbf{r},\mathbf{r}'} |\mathbf{r}\rangle V_{\mathbf{r},\mathbf{r}'}\langle\mathbf{r}'|, \qquad (5.11)$$

where $\mathcal{E}_{\mathbf{r}}$ is the on-site energy at lattice site $\mathbf{r}$, $V_{\mathbf{r},\mathbf{r}'}$ is the hopping energy between lattice sites $\mathbf{r}$ and $\mathbf{r}'$, and $\mathbf{r} = (m, n, l)$ is determined by the site indices. By using these site indices, we can write the state kets of the system as

$$|\mathbf{r}\rangle = |m\rangle|n\rangle|l\rangle. \qquad (5.12)$$

The commonly used assumption in the tight-binding model is that only the nearest neighbor interactions have to be taken into account. Furthermore it is convenient to represent the tight-binding Hamiltonian by using the second quantization (see appendix B): For each state $|\mathbf{r}\rangle$ there exists bosonic site annihilation and creation operators $\hat{a}_{\mathbf{r}}$ and $\hat{a}^{\dagger}_{\mathbf{r}}$, respectively. By using these

operators we get

$$\mathcal{H} = \sum_{\mathbf{r}} \mathcal{E}_{\mathbf{r}} \hat{a}^{\dagger}_{\mathbf{r}} \hat{a}_{\mathbf{r}} + \sum_{\mathbf{r},\mathbf{r}'} (V_{\mathbf{r},\mathbf{r}'} \hat{a}^{\dagger}_{\mathbf{r}} \hat{a}_{\mathbf{r}'} + V_{\mathbf{r}',\mathbf{r}} \hat{a}^{\dagger}_{\mathbf{r}'} \hat{a}_{\mathbf{r}}), \tag{5.13}$$

where $\mathbf{r}'$ represents nearest neighbors of $\mathbf{r}$.

The Green's functions for tight-binding Hamiltonian can, in general, be obtained by matrix inversion in the equation (5.8). Furthermore we can form the Green's functions for any $\mathbf{r}$ and $\mathbf{r}'$ by calculating the matrix elements

$$\mathbf{G}^{\pm}(\mathbf{r}, \mathbf{r}', \mathcal{E}) = \langle \mathbf{r} | \mathbf{G}^{\pm}(\mathcal{E}) | \mathbf{r}' \rangle. \tag{5.14}$$

It is sufficient to solve only $\mathbf{G}^{+}(\mathbf{r}, \mathbf{r}', \mathcal{E})$ because

$$\mathbf{G}^{-}(\mathbf{r}', \mathbf{r}, \mathcal{E}) = [\mathbf{G}^{+}(\mathbf{r}, \mathbf{r}', \mathcal{E})]^{*} \tag{5.15}$$

due to definition of $\mathbf{G}^{\pm}(\mathcal{E})$ i.e. equations (5.8) and (5.9).

For later use, the mixed representation is introduced: The longitudinal lattice location is presented by the lattice site index m while the transverse state is presented by the transverse mode numbers μ. Therefore matrix elements of the operator $\mathbf{G}$ can be written as

$$\mathbf{G}_{mm'}(\mathcal{E}) = \langle \mu, m | \mathbf{G}(\mathcal{E}) | m', \mu' \rangle. \tag{5.16}$$

These elements are also matrices with rank defined by the total number of modes.

5.4 Analytic lattice Green's functions

5.4.1 Finite 1D Tight-Binding Chain

Matrix Form of Green's function

Let us consider a finite one-dimensional tight-binding chain of N sites. In this special case the Hamiltonian can be written as

$$\mathcal{H} = \sum_{n} \mathcal{E}_n \hat{a}^{\dagger}_n \hat{a}_n + \sum_{n} (V_{n,n+1} \hat{a}^{\dagger}_n \hat{a}_{n+1} + V_{n+1,n} \hat{a}^{\dagger}_{n+1} \hat{a}_n), \tag{5.17}$$

where $n \in [1, N]$. The matrix form of the Hamiltonian (5.17) is

$$\mathcal{H} = \begin{bmatrix} \mathcal{E}_1 & V_{1,2} & & & & & \\ V_{2,1} & \mathcal{E}_2 & V_{2,3} & & & & \\ & V_{3,2} & \mathcal{E}_3 & V_{3,4} & & & \\ & & \ddots & \ddots & \ddots & & \\ & & & V_{N_1,N-2} & \mathcal{E}_{N-1} & V_{N-1,N} \\ & & & & V_{N,N-1} & \mathcal{E}_N \end{bmatrix}, \tag{5.18}$$

where only the nonzero elements are shown. The matrix form of the Green's function corresponding to the Hamiltonian (5.17) is given by equation (5.8) as follows:

$$\begin{aligned} \mathbf{G}^{\pm}(\mathcal{E}) &= [(\mathcal{E} \pm i\eta)\mathcal{I} - \mathcal{H}]^{-1} \qquad (5.19) \\ &= \begin{bmatrix} \mathcal{E}'_1 & -V_{1,2} & & & & \\ -V_{2,1} & \mathcal{E}'_2 & -V_{2,3} & & & \\ & \ddots & \ddots & \ddots & & \\ & & -V_{N_1,N-2} & \mathcal{E}'_{N-1} & -V_{N-1,N} \\ & & & -V_{N,N-1} & \mathcal{E}'_N \end{bmatrix}^{-1}, \end{aligned}$$

where $\mathcal{E}'_n = \mathcal{E} - \mathcal{E}_n \pm i\eta$.

Solving the tight-binding Hamiltonian is equivalent to solving the Schrödinger equation for a free particle in the hard wall boundaries by using the finite difference method. Thus the hopping energies V between adjacent sites and the on-site energies $\mathcal{E}_n$ are chosen so that the continuous and discretized problems give the same zero of energies. The values are [20]:

$$V = -\frac{\hbar^2}{2m^*\delta^2} \tag{5.20}$$

$$\mathcal{E}_n = -2V = \frac{\hbar^2}{m^*\delta^2}, \tag{5.21}$$

where δ is the grid spacing.

Analytic Forms of Green's function

The Green's function for finite tight-binding chain (of N lattice sites) can also be written in analytical form. The analytical Green's functions between the endpoints of the lattice are [20]:

$$\mathbf{G}_{11} = \frac{\sin(N\theta)}{V\sin[(N+1)\theta]} \tag{5.22}$$

$$\mathbf{G}_{1N} = \frac{\sin(\theta)}{V\sin[(N+1)\theta]}. \tag{5.23}$$

The θ in equations (5.22)-(5.23) is a function of propagation energy $\mathcal{E}$ and it is different for propagating and evanescent modes [20]:

$$\theta_{prop} = \arccos\left(\frac{\mathcal{E}}{2V}+1\right) \tag{5.24}$$

$$\theta_{evan} = i\cosh^{-1}\left(\frac{\mathcal{E}}{2V}+1\right), \tag{5.25}$$

where the first one is for propagating modes and the latter one is for evanescent modes.

5.4.2 Green's Function for Semi-Infinite Chain

In the semi-infinite tight-binding lattice, with the lattice sites $n = 1, \ldots, \infty$ (or equivalently $n = -1, \ldots, -\infty$), the Green's function cannot be represented in matrix form due to the infinite size of lattice. The analytical forms of the Green's function in the semi-infinite lattice are [20]:

$$\mathbf{G}_{11} = \frac{e^{i\theta}}{V} \tag{5.26}$$

$$\mathbf{G}_{1n} = \frac{e^{i|n|\theta}}{V} \tag{5.27}$$

$$\mathbf{G}_{nn} = \frac{e^{i|n|\theta}}{V}\frac{\sin(|n|\theta)}{\sin(\theta)}, \tag{5.28}$$

where θ is defined in equations (5.24)-(5.25) and it must be positive for $n = -1, \ldots, -\infty$.

5.5 Recursive Green's Function Method

In the recursive Green's function method [17, 21, 20] the entire lattice is divided into uniform subsections with a constant potential, whose Green's functions can be solved exactly. Let us denote the Hamiltonian of the isolated sections (i.e. the unperturbed Hamiltonian) by $\mathcal{H}_0$. Furthermore the coupling between each pair of isolated sections is taken as perturbation. It is denoted by V and defined as [20]

$$V = -\frac{\hbar^2}{2m^* a^2}, \tag{5.29}$$

where a is the lattice constant. Thus the total Hamiltonian is

$$\mathcal{H} = \mathcal{H}_0 + V. \tag{5.30}$$

Let us further assume that the Green's functions $\mathbf{G}^0$ of separate regions are known. Then the Green's function of a system consisting of the connected regions can be calculated from Green's functions $\mathbf{G}^0$ of individual slices by using the Dyson's equation

$$\mathbf{G} = \mathbf{G}^0 + \mathbf{G}^0 V \mathbf{G}, \tag{5.31}$$

where $\mathbf{G}$ is the total Green's function, $\mathbf{G}^0$ is the Green's function of single subsections and V is a small perturbation, which describes the nearest neighbor hopping between two adjacent sections.

From now on the earlier discussed mixed representation for Green's function is used: In the propagation direction each index $i, j, \ldots$ represents transverse slice and the transverse slice is represented by its transverse modes $\mu, \nu, \ldots$. Thus matrix $\mathbf{G}_{ij}$ denotes Green's functions from site i to site j and its matrix elements

$$\langle \mu | \mathbf{G}_{ij} | \nu \rangle = (\mathbf{G}_{ij})_{\mu\nu} = \langle \mu, i | \mathbf{G} | \nu, j \rangle \tag{5.32}$$

correspond to mode μ at site i and mode ν at site j.

Let us now consider the system shown in figure 5.1. The uniform region A from site i to site j is connected via the hopping interaction V to uniform

section B which goes from site k to site l. Green's functions $\mathbf{G}^A$ for region A must be known exactly but $\mathbf{G}^B$ for region B can also be calculated from Dyson's equations previous iteration steps.

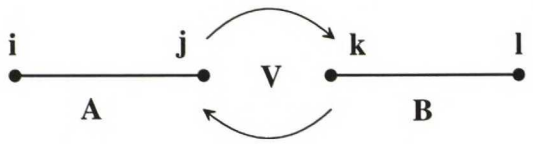

Figure 5.1: Schematic picture of sections of recursive Green's function method. Sections A and B are connected via hopping interaction V.

Let us now apply the Dyson's equation. We get

$$\begin{aligned}
\mathbf{G}_{il} &= \langle i|\mathbf{G}|l\rangle \\
&= \langle i|\mathbf{G}^0|l\rangle + \langle i|\mathbf{G}^0 V\mathbf{G}|l\rangle \\
&= \langle i|\mathbf{G}^0|l\rangle + \sum_{m,n}\langle i|\mathbf{G}^0|m\rangle\langle m|V|n\rangle\langle n|\mathbf{G}^0|l\rangle \\
&= \langle i|\mathbf{G}^0|j\rangle\langle j|V|k\rangle\langle k|\mathbf{G}^0|l\rangle \\
&= \mathbf{G}_{ij}V_{jk}\mathbf{G}_{kl}, \qquad (5.33)
\end{aligned}$$

where perturbation V acts only between sites j and k, and $\mathbf{G}^0$ are defined only in isolated sections. Similarly for $\mathbf{G}_{ii}$:

$$\begin{aligned}
\mathbf{G}_{ii} &= \langle i|\mathbf{G}|i\rangle \\
&= \langle i|\mathbf{G}^0|i\rangle + \langle i|\mathbf{G}^0 V\mathbf{G}|i\rangle \\
&= \langle i|\mathbf{G}^0|i\rangle + \sum_{m,n}\langle i|\mathbf{G}^0|m\rangle\langle m|V|n\rangle\langle n|\mathbf{G}^0|i\rangle \\
&= \langle i|\mathbf{G}^0|i\rangle + \langle i|\mathbf{G}^0|j\rangle\langle j|V|k\rangle\langle k|\mathbf{G}^0|i\rangle \\
&= \mathbf{G}^0_{ii} + \mathbf{G}_{ij}V_{jk}\mathbf{G}_{ki}. \qquad (5.34)
\end{aligned}$$

We are interested in $\mathbf{G}_{il}$ and $\mathbf{G}_{ii}$ because with those the transmission and reflection parameters can be calculated as will be seen later. By taking the elements of the Green's function $\mathbf{G}^{A+B}$ of the connected system (superscripts A and B denote the Green's functions of the isolated sections and superscript

$A + B$ denote the whole system), we get the following system of matrix equations

$$\mathbf{G}_{il}^{A+B} = \mathbf{G}_{ij}^{A} V_{jk} \mathbf{G}_{kl}^{A+B} \tag{5.35}$$

$$\mathbf{G}_{kl}^{A+B} = \mathbf{G}_{kl}^{B} + \mathbf{G}_{kk}^{B} V_{kj} \mathbf{G}_{jl}^{A+B} \tag{5.36}$$

$$\mathbf{G}_{jl}^{A+B} = \mathbf{G}_{jj}^{A} V_{jk} \mathbf{G}_{kl}^{A+B}. \tag{5.37}$$

$$\mathbf{G}_{ii}^{A+B} = \mathbf{G}_{ii}^{A} + \mathbf{G}_{ij}^{A} V_{jk} \mathbf{G}_{ki}^{A+B} \tag{5.38}$$

$$\mathbf{G}_{ki}^{A+B} = \mathbf{G}_{kk}^{B} V_{kj} \mathbf{G}_{ji}^{A+B} \tag{5.39}$$

$$\mathbf{G}_{ji}^{A+B} = \mathbf{G}_{ji}^{A} + \mathbf{G}_{jj}^{A} V_{jk} \mathbf{G}_{ki}^{A+B} \tag{5.40}$$

Substitution of equation (5.37) into equation (5.36) and equation (5.40) into equation (5.39) gives

$$\mathbf{G}_{kl}^{A+B} = [\mathcal{I} - \mathbf{G}_{kk}^{B} V_{kj} \mathbf{G}_{jj}^{A} V_{jk}]^{-1} \mathbf{G}_{kl}^{B} \tag{5.41}$$

$$\mathbf{G}_{ki}^{A+B} = [\mathcal{I} - \mathbf{G}_{kk}^{B} V_{kj} \mathbf{G}_{jj}^{A} V_{jk}]^{-1} \mathbf{G}_{kk}^{B} V_{kj} \mathbf{G}_{ji}^{A}. \tag{5.42}$$

Thus the substitution of equation (5.41) into equation (5.35) and the substitution of equation (5.42) into equation (5.38) gives $\mathbf{G}_{il}^{A+B}$ and $\mathbf{G}_{ii}^{A+B}$, respectively:

$$\mathbf{G}_{il}^{A+B} = \mathbf{G}_{ij}^{A} V_{jk} [\mathcal{I} - \mathbf{G}_{kk}^{B} V_{kj} \mathbf{G}_{jj}^{A} V_{jk}]^{-1} \mathbf{G}_{kl}^{B} \tag{5.43}$$

$$\mathbf{G}_{ii}^{A+B} = \mathbf{G}_{ii}^{A} + \mathbf{G}_{ij}^{A} V_{jk} [\mathcal{I} - \mathbf{G}_{kk}^{B} V_{kj} \mathbf{G}_{jj}^{A} V_{jk}]^{-1} \mathbf{G}_{kk}^{B} V_{kj} \mathbf{G}_{ji}^{A}. \tag{5.44}$$

This procedure is continued until each section is included in the total Green's function. In the first iteration B and correspondingly in the last iteration A must be perfect semi-infinite leads because they model electron reservoirs [17]. In other iteration steps A is a finite uniform lead and B is previously iterated sections. When the Greens function of the whole system is obtained, the transmission and reflection coefficients can be calculated from $\mathbf{G}_{il}$ and $\mathbf{G}_{ii}$ as will be seen in the next section.

5.6 Transmission and Reflection Coefficients

The rigorous wave packet analysis of the relation between Green's functions and the scattering matrix is represented in [22]. The transmission coefficient from mode μ at lattice site i into mode ν at lattice site l is [20]:

$$t_{\nu\mu} = -\mathrm{i}2V\sqrt{\sin(k_\nu a)\sin(k_\mu a)}e^{\mathrm{i}(k_\mu ai - k_\nu al)}\langle\mu|\mathbf{G}_{il}|\nu\rangle \tag{5.45}$$

and the reflection coefficients from mode μ at lattice site i back to the lattice site i into mode ν is [20]:

$$\begin{aligned} r_{\nu\mu} &= -\sqrt{\sin(k_\nu a)/\sin(k_\mu a)}e^{\mathrm{i}2(k_\nu + k_\mu)ai} \\ &\quad \cdot(\mathrm{i}2V\sin(k_\mu a)\langle\mu|\mathbf{G}_{ii}|\nu\rangle + \delta_{\nu\mu}). \end{aligned} \tag{5.46}$$

In the above equations k_μ is the wave vector available for longitudinal motion at transverse mode μ and a is the longitudinal distance between the lattice points i.e. the longitudinal grid spacing and $\mathrm{i} = \sqrt{-1}$.

5.7 Results of Calculations

5.7.1 T-Stub

The conductance of the same T-stub as in figure 4.2 was calculated by using the Green's function method as well as the mode matching method. The comparison of these methods is represented in figure 5.2. We see that the conductance curves are almost identical (note that the zero of the energy in figure 5.2 corresponds to a ground state energy $\mathcal{E}_1 \approx 75meV$).

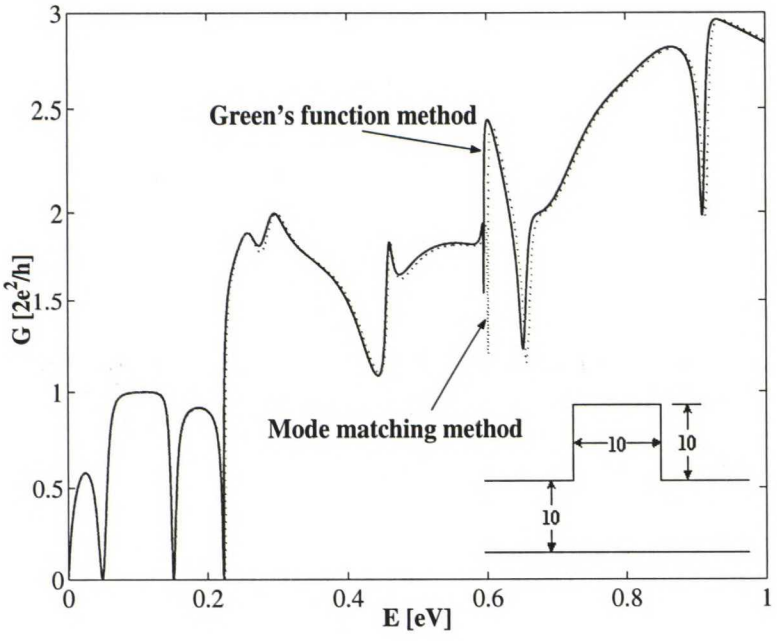

Figure 5.2: The conductance of the T-stub. The shape of the T-stub is shown in the inset. The waveguide is $w = 10\ nm$ wide and the size of the stub is $10\ nm \times 10\ nm$. The zero of the energy axis corresponds to the ground state energy of the lead: $\mathcal{E}(n = 1) = \hbar^2\pi^2n^2/(2m^*w^2) \approx 75\ meV$, $m^* = 0.05m_0$.

Chapter 6

Single Electron Tunneling

6.1 Introduction

A single electron circuit is based on one or more tunnel junction. The equivalent circuit of a tunnel junction has parallel connected capacitance C and resistance R_T. Theoretical studies as well as experimental tests have shown that a necessary condition for observing single electron charging effects is that the tunneling resistance is much higher than the quantum resistance i.e. $R_T \gg \frac{h}{e^2} \approx 25.8k\Omega$. This minimum tunnel resistance requirement suppresses the quantum mechanical uncertainty of electron location i.e. electrons need to be well localized on the islands.

If the junction is small and the insulator between the electrodes is not extremely thin, the capacitance of the tunnel junction is small and the charging energy

$$\mathcal{E}_C = \frac{e^2}{2C} \tag{6.1}$$

corresponding to a single electron can be as large as the Boltzmann constant times temperature ($k_B T$). Thus the charging energy is not negligible and the tunneling occurs only if the voltage V over the junction is large enough for the charging energy to be compensated by the energy of $e \times V$.

In nanometer scale systems the motion of electrons can be blocked by the charging energy. This phenomenon is called the Coulomb blockade.

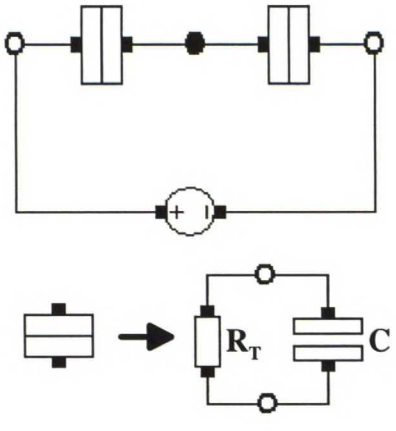

Figure 6.1: A picture of an island between tunnel junctions and the equivalent circuit of the tunnel junction.

The capacitance of the tunnel junction can be calculated from [23]:

$$C = \frac{\varepsilon A}{4\pi d}, \tag{6.2}$$

where ε is the dielectric constant of the highly resistive oxide layer, A is the junction area and d is the thickness of the oxide layer. The number of electrons in an island that is electrically isolated from the rest of the circuit, is an integer. The charging energy of a system depends on the amount of electrons in different parts of the system and on the applied voltages.

Single electronics is described by a model called the *Orthodox theory* in the literature. This theory is based on the following three assumptions [24, 17, 25, 26]:

1. The electron charging energy must be greater than the thermal energy $\mathcal{E}_{ch} > k_B T$. This conditions ensures that the electrons are well localized. It follows from Eq. 6.1 that to make single electronics observable at room temperature the capacitances must as low as $10^{-18} F$.

2. The charge relaxation time and the tunneling time (i.e. the time that an electron spends in the barrier) are assumed to be negligible small in comparison with other time scales (including the time interval between neighboring tunneling events). Furthermore it is assumed that the tunneling and relaxation are independent processes and that after tunneling the charge is relaxed before next tunneling event. The tunneling and relaxation times are of the order of few femtoseconds and few picoseconds, respectively.

3. Coherent quantum processes consisting of several simultaneous tunneling events ("co-tunneling" see e.g. [26, 17, 9, 27]) are ignored. This assumption is valid if the resistances R_T of all the tunnel barriers of the system is much higher than the quantum unit resistance $R_T \gg \frac{h}{e^2}$. This latter relation is of principal importance for single electronics as a whole because it also ensures that quantum fluctuations are negligible.

6.2 Elemental Single Electron Devices

6.2.1 Single Electron Box

Let us consider a single electron box (see figure 6.2), which consists of a small metallic island coupled via tunnel junction to an electrode and via the capacitor C_G to a gate voltage source. The capacitance of the tunnel junction is denoted by C_J and the resistance by R_T. If the gate voltage is zero, then the number of excess electrons in the island is zero at the lowest energy state of the system i.e. the system is charge neutral. Therefore this state is usually taken to be the reference state. For nonzero gate voltages the number of excess electrons in the island can change in discrete steps. This is a consequence of tunneling of electrons trough the junction.

The total excess charge in the box can be split into two parts Q_L and Q_R. Here Q_L is the charge related to capacitance C_J of tunnel junction whereas

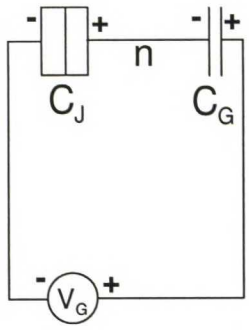

Figure 6.2: Single electron box

Q_R is the charge related to the capacitance C_G of the gate. Thus we can write $-ne = Q_L - Q_R$. According to the Kirchoff's law $V_G = Q_L/C_J - Q_R/C_G$. Furthermore the charging energy is $Q_L^2/2C_J + Q_R^2/2C_G$. By using $-ne = Q_L - Q_R$ the charging energy can be written as [26, 9]:

$$\mathcal{E}_{ch}(n, Q_G) = \frac{(ne - Q_G)^2}{2C_\Sigma}, \tag{6.3}$$

where $C_\Sigma = C_J + C_G$ and $Q_G = C_G V_G$. On the average the number of excess electrons in the island at the thermal equilibrium is given by [28]:

$$< n >= \sum_{n=-\infty}^{n=\infty} ne^{-\frac{\mathcal{E}_{ch}(n,Q_G)}{k_B T}} \Bigg/ \sum_{n=-\infty}^{n=\infty} e^{-\frac{\mathcal{E}_{ch}(n,Q_G)}{k_B T}}. \tag{6.4}$$

In figure 6.3 the charge of the electron box of circuit in figure 6.2 is plotted as a function of the gate voltage. All the following single electron circuit simulations were carried out by using a software called SIMON [29].

6.2.2 Single Electron Transistor

In the equivalent circuit of a single electron transistor (SET) an island is coupled via tunnel junctions to the source and drain and it is also capacitively coupled to the gate voltage V_G (see figure 6.4). The gate capacitor C_G is assumed to be ideal i.e. it has infinite tunnel resistance.

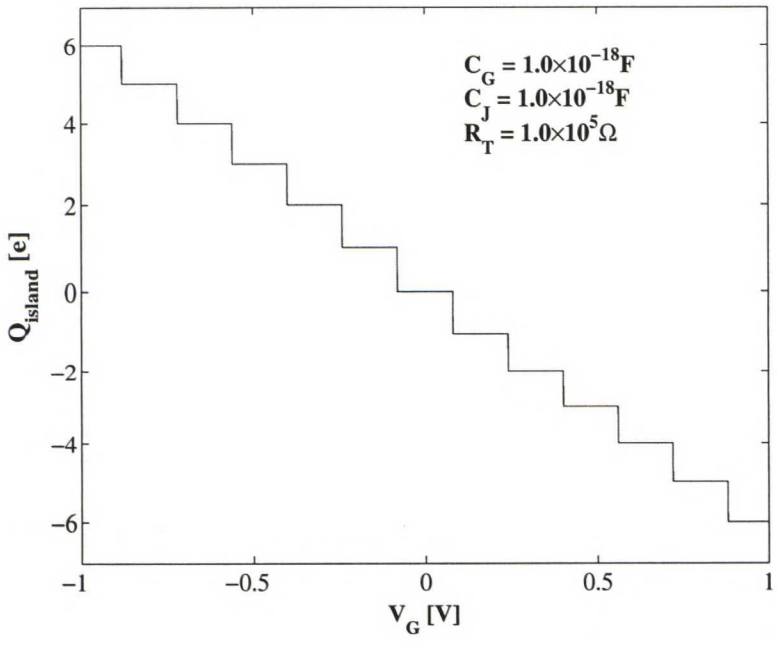

Figure 6.3: The charge of the single electron box as function of gate voltage at $T = 0K$. Note that $n = -Q_{\text{island}}/e$.

Let us denote the voltages of the left and the right tunnel junctions and the gate by V_L, V_R and V_G, respectively, and furthermore let V_0 denote the voltage at the island (see figure 6.4). An additional charge Q_G is produced to the island by the gate voltage:

$$Q_G = C_G(V_G - V_0). \tag{6.5}$$

Thus the charge in the island obeys equation

$$Q_R - Q_L - Q_G = -ne + Q_p, \tag{6.6}$$

where Q_p represents both the unintentional background polarization charge that usually exists in real structures due to the work-function differences and the random charges trapped near the junctions. The voltages across the tunnel junctions are [27]

$$V_L - V_0 = \frac{1}{C_\Sigma}[(C_G + C_R)V_L - C_G V_G - C_R V_R + ne - Q_p] \tag{6.7}$$

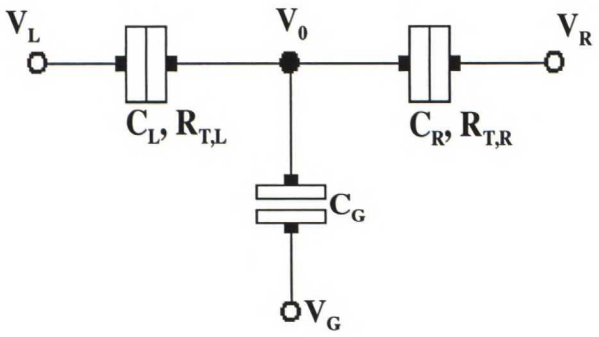

Figure 6.4: Single electron transistor

$$V_0 - V_R = \frac{1}{C_\Sigma}[C_L V_L + C_G V_G - (C_L + C_G)V_R - ne + Q_p], \quad (6.8)$$

where the equivalent capacitance C_Σ is a sum of all the capacitances:

$$C_\Sigma = C_L + C_R + C_G. \quad (6.9)$$

Furthermore the energy change of the system for tunnel events across left and right junctions are [27]

$$\Delta\mathcal{E}_L^\pm = \frac{e}{C_\Sigma}\Big(\frac{e}{2} \pm [(C_G + C_R)V_L - C_G V_G - C_R V_R + ne - Q_p]\Big) \quad (6.10)$$

$$\Delta\mathcal{E}_R^\pm = \frac{e}{C_\Sigma}\Big(\frac{e}{2} \pm [C_L V_L + C_G V_G - (C_L + C_G)V_R - ne + Q_p]\Big), \quad (6.11)$$

where the superscripts + and − correspond to forward and backward tunneling, respectively. At zero temperature only events that decrease the energy of the system are allowed i.e. $\Delta\mathcal{E}_{L,R}^\pm < 0$ (at higher temperatures thermal fluctuations in energy of the order of $k_B T$ weaken this condition). By setting $\Delta\mathcal{E}_{L,R}^\pm$ equal to zero we obtain the linear equations for the boundaries of the stable regions i.e. the coulomb blockades, where no current flows.

Let us assume that $C_L = C_R = C$, $T = 0K$ and that the gate voltage is zero and furthermore that the applied drain source voltage is below the threshold of tunneling $V_t = e/2C_\Sigma$ (see Eqs. (6.10) and (6.11)). Thus tunneling cannot

occur and no current flows due to Coulomb blockade which is a direct result of the additional Coulomb energy $e^2/(2C_\Sigma)$ that has to be gained by an electron in order to tunnel into or out of the island.

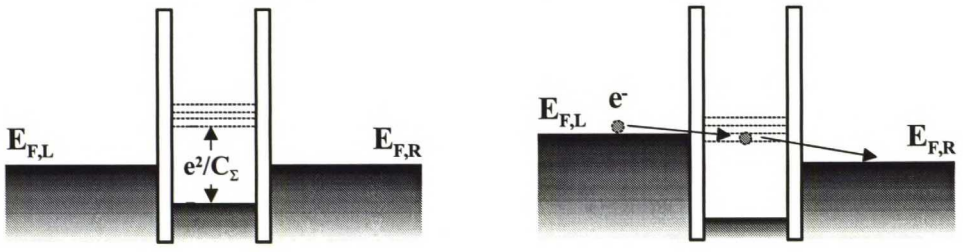

Figure 6.5: Energyband diagram of a double junction system. In the left figure all applied voltages are set to zero and no current flows through the SET. In the right figure electrons can tunnel into the island and out of it because the excited state of the island due to the Coulomb charging lies between the Fermi energies of the left and right leads.

When all applied voltages are set to zero (in analogy to the intrinsic semiconductors) one half of the Coulomb gap e^2/C_Σ, which has opened at the Fermi energy of the metal island, is below the original Fermi energy and one half is above it (see figure 6.5). Therefore there are no states available in the island for electrons to tunnel into from source or drain. Furthermore there is no empty states in the leads for electrons in the island to tunnel.

On the other hand if the applied bias voltage is over the threshold voltage an electron can tunnel from the source into the island raising the Fermi energy of the dot by e^2/C_Σ and preventing other electrons to tunnel until the applied bias voltage is over $3e/(2C)$ (cf. Eqs. (6.10) and (6.11)) or an electron is tunneled from island to the drain.

The gate voltage allows us to tune the device from one constant charge regime to another by adding one electron at the time into the island.

We can eliminate the offset charge Q_p by defining a new voltage $V_G' = V_G + Q_p/C_G$, because Q_p can be treated as an effective offset of the gate voltage.

In figure 6.6 the drain-source current and the charge of the single electron transistor in figure 6.4 is plotted as function of the gate voltage. This simulation was done by using SIMON.

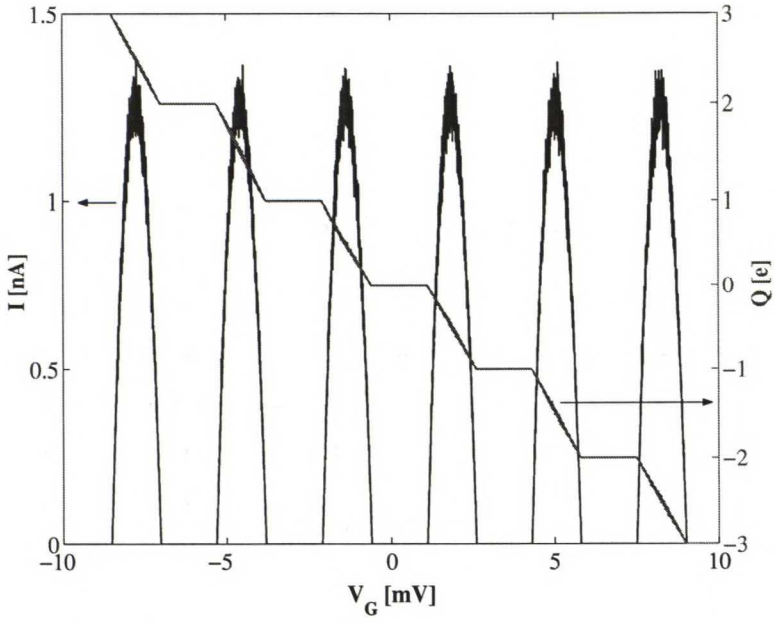

Figure 6.6: The drain-source current (the left vertical axis) and the charge of a metallic island (the right vertical axis) as a function of the gate voltage in SET at $T = 0K$. $R_{T,D} = R_{T,S} = 1.0 \cdot 10^5\Omega$, $C_D = C_S = C_G = 5.0 \cdot 10^{-17}F$ and $V_{DS} = 0.5mV$.

6.3 Transfer Hamiltonian Method

6.3.1 Single Junction

In the transfer Hamiltonian method the tunneling barrier is treated as a perturbation. The current can be calculated from the transfer rates of electrons which are obtained by using the time independent perturbation theory.

In the tunneling Hamiltonian approach the Hamiltonian operator is divided into three parts. On the left and right leads we have the unperturbed Hamil-

tonians $\mathcal{H}_L$ and $\mathcal{H}_R$, with known eigenvalues and eigenstates i.e. $\mathcal{H}_{L,R}\Psi_{L,R} = \mathcal{E}_{L,R}\Psi_{L,R}$. The total Hamiltonian is given by

$$\mathcal{H} = \mathcal{H}_L + \mathcal{H}_T + \mathcal{H}_R, \tag{6.12}$$

where $\mathcal{H}_T$ is the tunneling Hamiltonian. Let us now write these operators in the second quantized form by using the Fermionic annihilation and creation operators (see appendix B). The unperturbed Hamiltonians and the tunneling Hamiltonian in the second quantization form are

$$\mathcal{H}_0 = \mathcal{H}_L + \mathcal{H}_R = \sum_{\mathbf{k}_L} \mathcal{E}_{\mathbf{k}_L} \hat{a}^\dagger_{\mathbf{k}_L} \hat{a}_{\mathbf{k}_L} + \sum_{\mathbf{k}_R} \mathcal{E}_{\mathbf{k}_R} \hat{a}^\dagger_{\mathbf{k}_R} \hat{a}_{\mathbf{k}_R} \tag{6.13}$$

$$\mathcal{H}_T = \sum_{\mathbf{k}_L \mathbf{k}_R} T_{\mathbf{k}_L \mathbf{k}_R} \hat{a}^\dagger_{\mathbf{k}_R} \hat{a}_{\mathbf{k}_L} + \sum_{\mathbf{k}_L \mathbf{k}_R} T_{\mathbf{k}_R \mathbf{k}_L} \hat{a}^\dagger_{\mathbf{k}_L} \hat{a}_{\mathbf{k}_R}, \tag{6.14}$$

where $\mathcal{E}_{\mathbf{k}}$ is the energy of corresponding electronic state $\mathbf{k}$, and $T_{\mathbf{k}\mathbf{k}'}$ is the transmission probability between states $\mathbf{k}$ and $\mathbf{k}'$. In equations (6.13) and (6.14) the product of the creation ($\hat{a}^\dagger_{\mathbf{k}_{L,R}}$) and the annihilation ($\hat{a}_{\mathbf{k}_{L,R}}$) operators represents the occupation or the number operator

$$\hat{N}_{\mathbf{k}_{L,R}} = \hat{a}^\dagger_{\mathbf{k}_{L,R}} \hat{a}_{\mathbf{k}_{L,R}}. \tag{6.15}$$

For fermions the values of the number operators can only be zero or one. The expectation value of number operator gives the Fermi-Dirac distribution.

6.3.2 Hamiltonian for SET

The Hamiltonian operator for the whole single electron transistor (see figure 6.4) is given by

$$\mathcal{H} = \mathcal{H}_0 + \mathcal{H}_T = \mathcal{H}_L + \mathcal{H}_R + \mathcal{H}_I + \mathcal{H}_{ch} + \mathcal{H}_T, \tag{6.16}$$

where the Hamiltonians are [30, 31, 32]:

$$\mathcal{H}_L = \sum_{k,n} \mathcal{E}^L_{k,n} \hat{a}^\dagger_{L,k,n} \hat{a}_{L,k,n} \tag{6.17}$$

$$\mathcal{H}_R = \sum_{k,n} \mathcal{E}^R_{k,n} \hat{a}^\dagger_{R,k,n} \hat{a}_{R,k,n} \tag{6.18}$$

$$\mathcal{H}_I = \sum_{q,n} \mathcal{E}^I_{q,n} \hat{c}^\dagger_{q,n} \hat{c}_{q,n} \tag{6.19}$$

$$\mathcal{H}_{ch} = \frac{e^2}{2(C_L + C_R + C_G)} (\hat{N} - N_C)^2 \tag{6.20}$$

$$\mathcal{H}_T = \sum_{r=L,R} \sum_{k,q,n} T^{r,n}_{k,q} \hat{a}^\dagger_{r,k,n} \hat{c}_{q,n} + \sum_{r=L,R} \sum_{k,q,n} T^{r,n}_{q,k} \hat{c}^\dagger_{q,n} \hat{a}_{r,k,n}. \tag{6.21}$$

Above $\mathcal{H}_L$, $\mathcal{H}_R$ and $\mathcal{H}_I$ describe the noninteracting electrons in the left and right leads and in the island, respectively. Furthermore the index $n = 1, \ldots, N$ ($N \gg 1$ for metallic island) is the transverse channel index including the spin degeneracy and the wavevectors k and q numerate the eigenstates of the electrons within one channel. In $\mathcal{H}_{ch}$, which describes the Coulomb interaction of the electrons in the island, $\hat{N}$ denotes the excess electron number operator and eN_C represents the charge induced by the applied gate and transport voltages: $N_C = (C_L V_L + C_R V_R + C_G V_G)/e$. Thus N_C is the classical number of excess electrons in the SET and furthermore it is the charge that minimizes the electrostatic energy. The matrix elements $T^{r,n}_{k,q}$ in the tunneling Hamiltonian $\mathcal{H}_T$ are assumed to be constants [9, 30, 27] and are related to the tunneling conductance of the junctions as follows

$$\frac{1}{R_{T,r}} = \frac{2\pi e^2}{\hbar} N_{r0} N_{I0} |T^r|^2, \tag{6.22}$$

where N_{r0} and N_{I0} are the density of states functions at the Fermi level in leads and island, respectively, and $r = L, R$.

6.4 Transition Rate

Let us denote the energy change of the system for tunneling events across the junction r ($= L, R$) by $\Delta\mathcal{E}^\pm_r$ as before (see equations (6.10)-(6.11)), where $\pm$ signs refers to the forward and reverse tunneling, respectively. The tunneling rate can be written by using the Fermi golden rule as follows:

$$\Gamma_r(\Delta\mathcal{E}^\pm_r) = \frac{2\pi}{\hbar} \sum_{i,f} |T^r_{\mathbf{k}_i,\mathbf{k}_f}|^2 f(\mathcal{E}_i)[1 - f(\mathcal{E}_f)] \delta(\mathcal{E}_i - \mathcal{E}_f - \Delta\mathcal{E}^\pm_r), \tag{6.23}$$

where i and f represents the initial and final states, respectively. Furthermore the argument of the δ-function includes the total energy change caused by the single electron tunneling. The usual approximation is that the variation of the tunnel transmission coefficient is assumed to be negligible. Thus $|T^r_{\mathbf{k}_i,\mathbf{k}_f}|^2 \equiv |T^r|^2$ can be taken outside of the summation in equation (6.23). Next we want to convert the sums over momentum in equation (6.23) to integrals over energy. In a small energy interval $\mathrm{d}\mathcal{E}$ the number of electron states is given by $N(\mathcal{E})\mathrm{d}\mathcal{E}$. Thus the transition rate can be written as

$$\begin{aligned}\Gamma_r(\Delta\mathcal{E}_r^{\pm}) &= \frac{2\pi}{\hbar}|T^r|^2 \int_{\mathcal{E}_{c,i}}^{\infty}\int_{\mathcal{E}_{c,f}}^{\infty} N_i(\mathcal{E}_i)N_f(\mathcal{E}_f) \\ &\quad \times f(\mathcal{E}_i)[1-f(\mathcal{E}_f)]\delta(\mathcal{E}_i-\mathcal{E}_f-\Delta\mathcal{E}_r^{\pm})\mathrm{d}\mathcal{E}_f\mathrm{d}\mathcal{E}_i, \qquad (6.24)\end{aligned}$$

where $\mathcal{E}_{c,i}$ is the conduction band edge of the side where electron resides initially and $\mathcal{E}_{c,f}$ is the conduction band edge of the side the electron is tunneling to, furthermore $N_i(\mathcal{E}_i)$ and $N_f(\mathcal{E}_f)$ are the density of states functions for the initial and final sides, respectively. The density of states functions can be taken as constants because the main contribution of the integral comes from narrow energy range around the Fermi energies which is defined by the product of the two Fermi-Dirac distribution functions. After integrating the δ-function the transition rate becomes

$$\Gamma_r(\Delta\mathcal{E}_r^{\pm}) = \frac{2\pi}{\hbar}|T^r|^2 N_i N_f \int_{\mathcal{E}_c^m}^{\infty} f(\mathcal{E})[1-f(\mathcal{E}-\Delta\mathcal{E}_r^{\pm})]\mathrm{d}\mathcal{E}, \qquad (6.25)$$

where $\mathcal{E}_c^m$ is the bigger of the two conduction band minima $\mathcal{E}_{c,i}$ and $\mathcal{E}_{c,f}$. For metallic tunnel junction $\mathcal{E}_F \gg \mathcal{E}_c$. Thus the integral in equation (6.25) can be approximated as follows:

$$\begin{aligned}&\int_{-\infty}^{\infty} f(\mathcal{E})[1-f(\mathcal{E}-\Delta\mathcal{E})]\mathrm{d}\mathcal{E} = \int_{-\infty}^{\infty}\frac{f(\mathcal{E})-f(\mathcal{E}-\Delta\mathcal{E})}{1-e^{\Delta\mathcal{E}/(k_BT)}}\mathrm{d}\mathcal{E} \\ &= -\frac{k_BT}{1-e^{\Delta\mathcal{E}/(k_BT)}}\Big|_{-\infty}^{\infty} \ln\left(\frac{1+e^{-\frac{\mathcal{E}-\mathcal{E}_F}{k_BT}}}{1+e^{-\frac{\mathcal{E}-\Delta\mathcal{E}-\mathcal{E}_F}{k_BT}}}\right) = \frac{\Delta\mathcal{E}}{1-e^{\frac{\Delta\mathcal{E}}{k_BT}}}. \qquad (6.26)\end{aligned}$$

By using the above result and the expression of the tunneling resistance (equation (6.22)) we obtain

$$\Gamma_r(\Delta\mathcal{E}_r^{\pm}) = \frac{\Delta\mathcal{E}_r^{\pm}}{e^2R_{T,r}(e^{\frac{-\Delta\mathcal{E}_r^{\pm}}{k_BT}}-1)}. \qquad (6.27)$$

At low temperatures $|\Delta\mathcal{E}_r^{\pm}| \gg k_B T$ and the transition rates are reduced to

$$\begin{cases} \Gamma_r(\Delta\mathcal{E}_r^{\pm}) &= -\frac{1}{e^2 R_{T,r}}\Delta\mathcal{E}_r^{\pm} \quad \text{for} \quad \Delta\mathcal{E}_r^{\pm} < 0 \\ \Gamma_r(\Delta\mathcal{E}_r^{\pm}) &= 0 \qquad\qquad\quad \text{for} \quad \Delta\mathcal{E}_r^{\pm} \geq 0. \end{cases} \tag{6.28}$$

6.5 Master Equation Approach

6.5.1 Single Island

Let us assume that the tunneling rates between the left lead and the island ($\Gamma_L^{\pm}$) and between the right lead and the island ($\Gamma_R^{\pm}$) (+ signs correspond to the electron tunneling into an island) are known (see figure 6.4). Furthermore, let $p(n,t)$ represent the probability to find the island in a state n at time t. Hence the Master equation can be written as

$$\begin{aligned} \frac{\partial}{\partial t}p(n,t) &= -[\Gamma_L^+(n) + \Gamma_L^-(n) + \Gamma_R^+(n) + \Gamma_R^-(n)]p(n,t) \\ &\quad +[\Gamma_L^+(n-1) + \Gamma_R^+(n-1)]p(n-1,t) \\ &\quad +[\Gamma_L^-(n+1) + \Gamma_R^-(n+1)]p(n+1,t). \end{aligned} \tag{6.29}$$

The first row on the right hand side of the equation (6.29) corresponds to the transitions from the state n to the state $n \pm 1$. It represents processes which remove the system away from the state n and has therefore negative sign. The second row of (6.29) corresponds to a transition from the state $n-1$ to the state n and the last row a transition from the state $n+1$ to the state n. These rows represent processes which bring the system to the state n and hence have positive signs.

Current trough the tunnel junction can now be calculated using the known values of the transition rates and probabilities. The current is obtained by summing over all the possible states:

$$I_{L,R}(t) = -e\sum_n p(n,t)[\Gamma_{L,R}^+(n) - \Gamma_{L,R}^-(n)]. \tag{6.30}$$

When the applied voltages are direct-current voltages only the stationary solution (i.e. equation (6.29) is set equal to zero) of master equation is needed and $I = I_L = I_R$.

6.5.2 System of Tunneling Junctions

The master equation approach of the previous section can easily be extended to the case of M islands. Let $p(n_1, n_2, \ldots, n_M, t)$ denote the normalized probability to find the system in a state, where island i has an occupancy n_i. Then the master equation for the system can be written as follows [33]:

$$\begin{aligned}\frac{\partial p(n_1, n_2, \ldots, t)}{\partial t} = \sum_{j=1,M} \Big[& \Gamma_j^+(n_1, \ldots, n_j - 1)p(n_1, \ldots, n_j - 1, \ldots, t) \\ & + \Gamma_j^-(n_1, \ldots, n_j + 1)p(n_1, \ldots, n_j + 1, \ldots, t) \\ & - \Gamma_j^+(n_1, \ldots, n_j)p(n_1, \ldots, n_j, \ldots, t) \\ & - \Gamma_j^-(n_1, \ldots, n_j)p(n_1, \ldots, n_j, \ldots, t)\Big]. \end{aligned} \tag{6.31}$$

In the above equation the tunneling rates are obtained from (6.27) by setting $\Delta\mathcal{E}$ as a change in the free energy during a corresponding tunneling event.

6.6 Monte Carlo Method

Numerical methods that involve sampling of random numbers are called Monte Carlo methods (see e.g. [34, 35, 36]). These simulation methods are common in engineering. In the following Monte Carlo (MC) method is used in the simulations of single electron circuits [27, 37, 38, 24]. The MC methods are very effective in simulations of single electron tunneling effects because of the strong quantum confinement of electrons in the islands. This allows the tunneling of electrons to be modeled accurately as discrete events. The probability that a tunneling event occurs exactly at the time t is obtained from the Poisson distribution

$$p(t) = e^{-\Gamma t}, \tag{6.32}$$

where Γ is the transition rate (see equation(6.27)). Thus the times t of the tunneling events are obtained from evenly distributed random numbers r by

taking the inverse of distribution function (6.32) as follows:

$$t = -\frac{\ln(r)}{\Gamma}, \tag{6.33}$$

where $0 < r \leq 1$.

The schematic flow chart of the MC method is represented in figure 6.7. The algorithm of the method consists of the following steps [27]:

1. Form the capacitance matrix $\mathbf{C}$ of the circuit. C_{ii} represent the total capacitance of conductor i and C_{ij} is the negative capacitance between conductors i and j, $(i, j \in [1, N])$.

2. Calculate for each possible tunnel event:

   - Free energy change (for constant temperature)
     $\Delta F = F_f - F_i = U_f - U_i + W_i - W_f$, where
     $W = \sum_{\text{sources}} \int V(t)I(t)\mathrm{d}t$ and
     $U = \frac{1}{2}\sum_{i=1}^{N}\sum_{j=1}^{N} C_{ij}^{-1} q_i q_j$, $(C_{ij}^{-1} = (\mathbf{C}^{-1})_{ij})$.
   - Tunneling rate
     $\Gamma(\Delta F) = \frac{\Delta F}{e^2 R_T (e^{\Delta F/(k_B T)} - 1)}$

3. Calculate the exit tunnel time, $t_{exit} = -\frac{\ln(r_1)}{\sum_i \Gamma_{ik}}$, out of the current state k. ($r_1 \in (0, 1]$ is evenly distributed random number)

4. Let r_2 be an evenly distributed random number and $r_2 \in [0, \sum_i \Gamma_{ik}]$. Select the winning event n that actually happens. The condition for n to be the winning event is $\sum_{i=1}^{n-1} \Gamma_{ik} < r_2 < \sum_{i=1}^{n} \Gamma_{ik}$.

5. Update node charges
   $q_i = \sum_{j=1}^{N} C_{ij} v_j$, where v_j is the potential of node j.

6. If the ending conditions (time, accuracy and event limits) are reached, terminate calculations. Otherwise go back to 2.

The number of events must be large enough to ensure that equilibrium is reached. Let us assume that there is very large capacitance C_{max} in the circuit and that the applied voltage over the capacitance is altered with small discrete steps ΔV. Thus the capacitor has to be charged by $C_{max}\Delta V$, which means that at least $C_{max}\Delta V/e$ tunneling events have to be simulated. In reality more events must be taken into simulations because events will happen elsewhere in the circuit too.

6.7 Higher-Order Effects

The orthodox theory presented previously in this chapter neglects many second order effects. In the following we briefly list the most prominent higher order effects because for a complete single electron device analysis some of these effects can be important.

6.7.1 Co Tunneling

The transition rate in section 6.4 was derived from the first order perturbation theory. In the Coulomb blockade regime, where the first order transition rate is low (or even zero at zero temperature), the higher order tunneling (co tunneling, [27, 39, 9, 26]) processes may become important, especially when the tunnel resistance is small and close to the fundamental resistance e^2/h.

Let us consider a system of two tunnel junctions. A second-order tunneling is possible for bias voltages V_b below the Coulomb blockade because the change in the free energy for a tunneling process trough the whole two junction system is negative, although the change in the free energy for independent tunneling in either tunneling junctions is positive. The change in the free energy is $-eV_b$, because the electron is transferred trough the whole bias voltage drop.

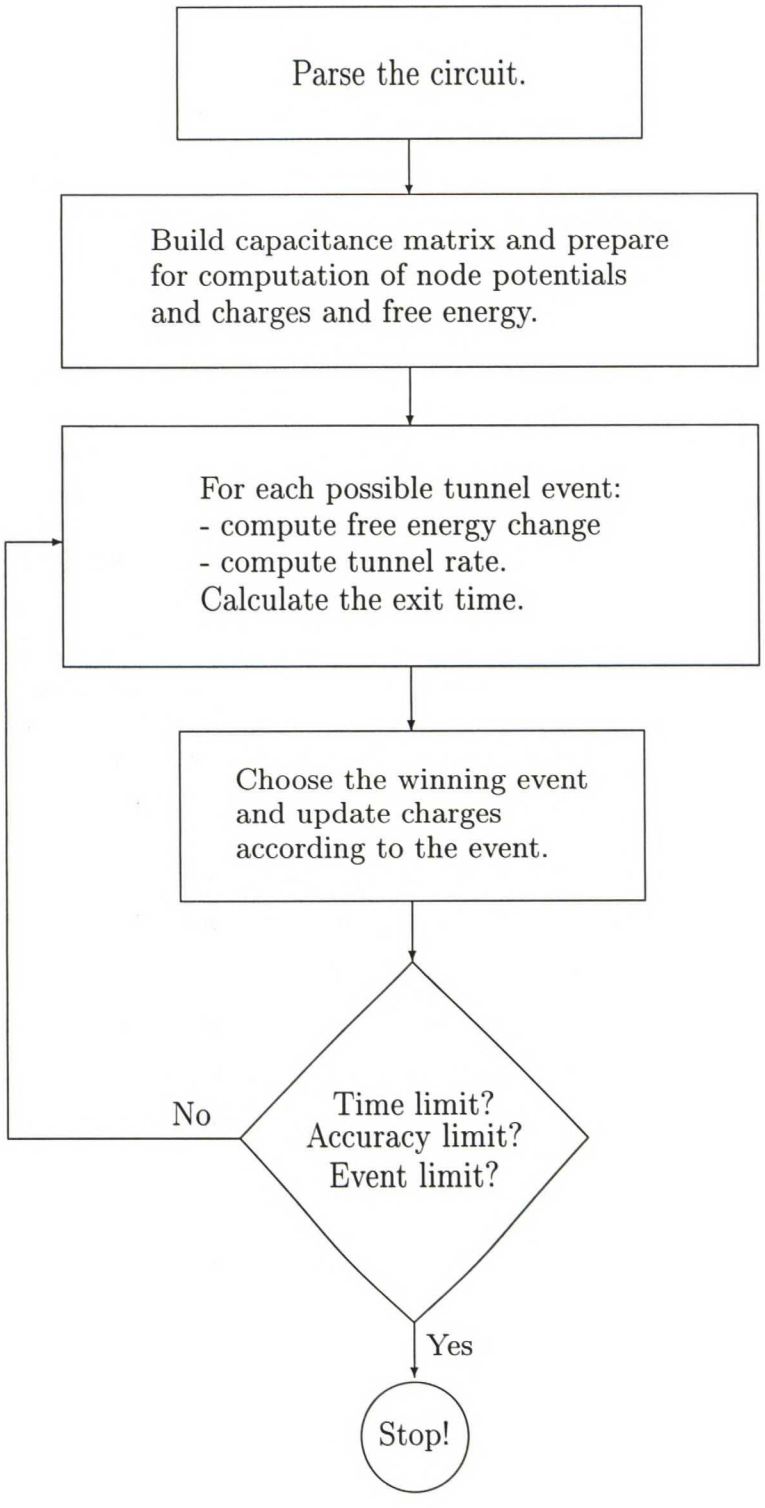

Figure 6.7: Flow chart of the Monte Carlo method.

The second-order co tunneling rate is given by [26]:

$$\Gamma^{(2)} = \frac{2\pi}{\hbar}|T_1|^2|T_2|^2\Big|\frac{1}{\Delta F_1} + \frac{1}{\Delta F_2}\Big|^2\delta(\mathcal{E}_i - \mathcal{E}_f). \tag{6.34}$$

In practice for a system of N junctions in series the Nth order co tunneling can be important in suitable circumstances. The rate for this tunneling event is [27]:

$$\begin{aligned}\Gamma^{(N)} &= \frac{2\pi}{\hbar}\Big(\prod_{i=1}^{N}\frac{\hbar}{2\pi e^2 R_{Ti}}\Big)\int\Big|\sum_{\mathrm{p}(k_1,\ldots,k_N)}\prod_{k=1}^{N-1}\frac{1}{\Delta F_k + \sum_{l=1}^{k}\omega_{2l-1} + \omega_{2l}}\Big|^2 \\ &\times\ \delta\Big(\Delta F_N + \sum_{i=1}^{2N}\omega_i\Big)\prod_{i=1}^{2N}(1 - f(\omega_i))\mathrm{d}\omega,\end{aligned} \tag{6.35}$$

where ω_x are the intermediate energy levels to and from which the electrons tunnel, $\mathrm{p}(k_1,\ldots,k_N)$ denotes all permutations of numbers $k_1,\ldots,k_N$ and $\Delta F_x = F_x - F_0$. Furthermore F_0 is the energy level from which Nth order co tunneling process starts.

6.7.2 Electro-Magnetic Environment

The orthodox theory assumes that charges relax instantaneously i.e. the charge imbalance caused by the tunneled electron reaches immediately the equilibrium configuration. This would be a good assumption for strictly capacitive circuits, but that is not the case if also resistors and/or inductors are present. There are two theories which take the electro-magnetic environment into account:

The Quantum Langvevin Theory couples the thermal noise of normal resistors to charge fluctuations at tunnel junctions. The effective tunnel rate under the influence of electro-magnetic environment is obtained by convoluting the transition rate (6.27) with the probability distribution of the charge fluctuations [27]:

$$<\Gamma^{\pm}(Q)> \;=\; \int_{-\infty}^{\infty}\Gamma(Q+q)\frac{1}{\sqrt{2\pi <q^2>}}e^{-\frac{q^2}{2<q^2>}}\mathrm{d}q$$

$$= \frac{1}{eR_TC\sqrt{2\pi < q^2 >}} \times \int_{-\infty}^{\infty} \frac{-\frac{e}{2} \mp Q - q}{1 - e^{e(e/2 \pm Q + q)/(Ck_BT)}} e^{-\frac{q^2}{2<q^2>}} \mathrm{d}q, \quad (6.36)$$

where

$$< q^2 >= \int_{-\infty}^{\infty} \frac{\frac{\hbar\omega R}{\pi} \coth(\frac{\hbar\omega}{2k_BT})}{(C_E^{-1} + C^{-1} - L_E\omega^2)^2 + R_E^2\omega^2} \mathrm{d}\omega. \quad (6.37)$$

The subscript E denotes the electro-magnetic environment that is connected to tunnel junction.

The Phase Correlation Theory models the tunnel junction capacitance and its electro-magnetic environment with infinite number of harmonic oscillators and accounts for the tunneling as a perturbation. The tunneling rate in the phase correlation theory is [27, 26, 9]:

$$\Gamma(\Delta F) = \frac{1}{e^2R_T} \int_{-\infty}^{\infty} \frac{\mathcal{E}}{1 - e^{-\mathcal{E}/(k_BT)}} \frac{1}{h} \int_{-\infty}^{\infty} \times e^{\frac{2e^2}{h} \int_{-\infty}^{\infty} \frac{\Re(Z_t(\omega))}{\omega} \frac{e^{-j\omega t} - 1}{1 - e^{-\hbar\omega/(k_BT)}} \mathrm{d}\omega - i(\mathcal{E} + \Delta F)t/\hbar} \mathrm{d}t\mathrm{d}\mathcal{E}, \quad (6.38)$$

where $Z_t(\omega)$ is the total impedance seen by the tunneling electron.

6.7.3 Alternating Density of States

In the derivation of tunneling rate it was assumed that the density of states function is constant $N(\mathcal{E}) \equiv N_0$, where N_0 denotes the density of states at the Fermi level. In materials with a bandgap (such as semiconductors and superconductors) more accurate analysis requires that the energy dependence of DOS is taken into account. The density of states functions for different material types are [27]:

$$N_{\text{metal}}(\mathcal{E}) = N_0 \quad (6.39)$$

$$N_{\text{semic.}}(\mathcal{E}) = \begin{cases} \frac{(2m_e^*)^{3/2}}{2\pi^2\hbar^3}\sqrt{\mathcal{E} - \mathcal{E}_c} & \mathcal{E} \geq \mathcal{E}_c \\ \frac{(2m_h^*)^{3/2}}{2\pi^2\hbar^3}\sqrt{\mathcal{E}_v - \mathcal{E}} & \mathcal{E} \leq \mathcal{E}_v \\ 0 & \mathcal{E}_v < \mathcal{E} < \mathcal{E}_c \end{cases} \quad (6.40)$$

$$N_{\text{superc.}}(\mathcal{E}) = \begin{cases} N_0 \frac{|\mathcal{E}-\mathcal{E}_F|}{\sqrt{(\mathcal{E}-\mathcal{E}_F)^2-\Delta}} & |\mathcal{E}-\mathcal{E}_F| > \Delta \\ 0 & |\mathcal{E}-\mathcal{E}_F| \leq \Delta. \end{cases} \tag{6.41}$$

In the above equations Δ is the half width of the superconducting gap [39].

In metals the Fermi energy is several eVs and approximately independent of temperature. Furthermore $\mathcal{E}_F \gg k_B T$ is a good approximation also at room temperature. Thus the Fermi-Dirac distribution function is close to a stepfunction also at room temperature and only electrons in the narrow energy range near the Fermi energy can be excited to higher states. Therefore the density of states in metals can be considered as constant: $N \equiv N(\mathcal{E}_F)$.

6.7.4 Superconducting Junctions

In a small temperature range near the critical temperature T_c, which is material constant, the electrical resistance of various metals completely vanish and the material become superconductor. The superconductivity causes several tunneling effects:

Quasiparticle Tunneling differ from the non-superconducting tunneling in that the density of states functions 6.41 must be used for the superconducting electrode(s).

Parity Effect [39, 27]takes place in tunnel junctions between normal and superconducting electrodes. The superconductor is in its ground state when all electrons near Fermi level are paired. If now a quasiparticle tunnels from normally conducting side into the superconductor, the state of the superconductor becomes excited with one extra electron. This unpaired electron has increased probability to tunnel out from the superconductor.

Andreev Reflections is a coherent second order process and it takes place in a tunnel junction between a normal- and superconductor [39, 27]. An electron coming from the normal side pulls another electron with it forming a Cooper pair [40, 39] into the superconductor.

Coherent Cooper Pair Tunneling [9, 27] is a process that is free of dissipation. The transferred charge is $2e$.

Incoherent Cooper Pair Tunneling is an event where the phase-coherence is destroyed e.g. by an external impedance $Z(\omega)$. The transition rate can be derived by using perturbation theory, but it has to be noted that the transferred charge is $2e$ instead of e. The tunneling rate is given by [9, 39]:

$$\begin{aligned}\Gamma &= \frac{\pi}{2\hbar}\left(\frac{h}{R_T \Delta 2e^2}\right)^2 \\ &\times \frac{1}{h}\int_{-\infty}^{\infty} e^{\frac{2e^2}{h}\int_{-\infty}^{\infty}\frac{\Re(Z_t(\omega))}{\omega}\frac{e^{-j\omega t}-1}{1-e^{-\hbar\omega/(k_B T)}}\mathrm{d}\omega + i\Delta F_{2e} t/\hbar}\mathrm{d}t, \end{aligned} \tag{6.42}$$

where ΔF_{2e} is the free energy change of the tunneling process of two electrons.

6.7.5 Self-Heating

The free energy difference which is released in the tunneling process must be dissipated for each tunnel event in either of the electrodes of the tunneling junction. Thus the tunneling electron thermalizes via the electron-electron interaction which is so fast process in metals that after the tunneling electron becomes instantly in thermal equilibrium. The self-heating induced by this fast relaxation process can cause different electron temperatures on different sides of the tunnel junction. This has to be taken into account in the tunneling rate [41, 27]:

$$\Gamma(\Delta F) = \frac{1}{e^2 R_T}\int_{-\infty}^{\infty} f(\mathcal{E}, T_i)(1 - f(\mathcal{E} - \Delta f, T_f))\mathrm{d}\mathcal{E}, \tag{6.43}$$

where T_i and T_f are temperatures of initial and final sides of the tunnel junction, respectively.

Electrons can also exchange energy with the lattice by emitting or absorbing phonons. However the electron phonon interaction is weak at low temperatures.

6.7.6 Polarization of Electrodes

The potential barrier is modified by the electrons that tunnel trough it because the tunneling charges polarize the electrodes. The polarization of the electrodes exert a force back on the electron. Effect of this force (or electric field) can be expressed by a potential which is a correction to the potential of the potential barrier. This effect can be taken into account by the image charge method [27, 42].

6.8 Array of Tunnel Junctions

By connecting several tunnel junctions in series and in parallel one obtains some advantages compared to single SET. The tunnel junction arrays are more tolerant to background charges and in the arrays it is easier to avoid stray capacitances and decouple the system from environment. Furthermore many of the single electron effects are more pronounced in tunnel junction arrays.

6.8.1 One-Dimensional Array

Let us consider an 1D array of N ($N \gg 1$) tunneling junctions. Let us furthermore, for simplicity, assume that the array is homogeneous i.e. the junctions are identical each having a capacitance C and a tunnel resistance R_T. The self capacitance of each island is C_0. An array with $N = 11$ tunnel junctions (10 islands) is plotted in figure 6.8. By assuming that other than the nearest neighbors coupling capacitances are negligible, the coupling capacitances can be written in a matrix form as follows:

$$C_{ij} = \begin{cases} C_0 & \text{for} \quad i = j \\ C & \text{for} \quad i = j \pm 1 \\ 0 & \text{for} \quad |i - j| > 1. \end{cases} \tag{6.44}$$

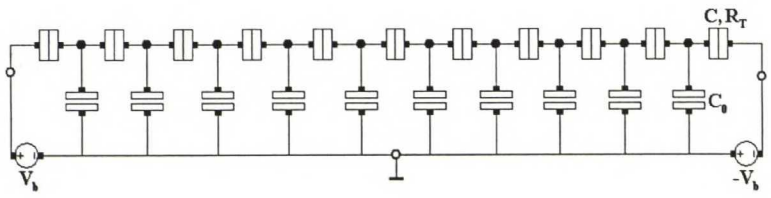

Figure 6.8: Schematic picture of 1D array of tunneling junctions with eleven equivalent tunneling junctions and ten islands.

Let us now assume that an electron is put into the jth island. Thus a potential $\phi_j = -e/C_{eff}$ will be generated. Here the effective capacitance is given by $C_{eff} = C_0 + 2C_h$, where C_h is the total capacitance of the half infinite array. The same capacitance is also seen from the next island so it can be written as

$$C_h = \frac{1}{C^{-1} + (C_0 + C_h)^{-1}} = \frac{1}{2}\left(\sqrt{C_0^2 + 4CC_0} - C_0\right). \tag{6.45}$$

Thereby the effective capacitance is given by

$$C_{eff} = \sqrt{C_0^2 + 4CC_0}. \tag{6.46}$$

At the arbitrary island i the potential caused by the charged island j is [43, 26]:

$$\phi_i = -\frac{e}{C_{eff}} e^{-\alpha|i-j|}, \tag{6.47}$$

where

$$\alpha = \ln\left(\frac{C_{eff} + C_0}{C_{eff} - C_0}\right). \tag{6.48}$$

The potential decays exponentially on both sides of island j. If the electron tunnels from the island j to $j \pm 1$, also the potential distribution will move one step to right or left (corresponding to $\pm$) keeping its from. This potential distribution is called a soliton. The range of the soliton is approximately $2\alpha^{-1}$ junctions. Similarly, if an electron is removed from the jth island, the result is an anti-soliton, which has the same form but an opposite sign. The energy of a soliton is $\mathcal{E}_S = e^2/(2C_{eff})$.

If large enough voltage is applied to the array, a single electron will eventually tunnel into the first island i.e. a soliton is injected into the array. The threshold voltage for the soliton to be injected is given by [26]:

$$V_t = \frac{e}{2C_{eff}}(1 + e^{-\alpha}) = \frac{e}{C_{eff} + C_0}. \tag{6.49}$$

When the applied bias exceeds V_t, solitons are injected into the array. Since they repeal each other, they start to move and create a current. If the other end of the array is biased with a voltage equal in magnitude but opposite in sign, then anti-solitons are injected into one end of the array and solitons into the other end of the array. Thus, when a soliton and an anti-soliton encounter at the middle of the array they annihilate. In the case of symmetric bias, the threshold voltage for the current is

$$V_S = 2V_t = \frac{2e}{C_{eff} + C_0} \approx \frac{2}{\sqrt{CC_0}}, \tag{6.50}$$

where the last form holds if the self capacitance is much smaller than the capacitances of the tunnel junctions i.e. if $C_0 \ll C$.

I-V curve of the 1D array with $N = 11$ tunnel junctions is presented in figure 6.9.

6.8.2 Two-Dimensional Array

A parallel coupling of 1D tunneling junction arrays forms a 2D tunnel junction array. 2D arrays are more reliable than 1D arrays because chain of arrays is only as good as the weakest link in it. Thus if one junction (and consequently the whole chain) breaks the other chains take over and the current continues to flow.

The length of the two-dimensional array determines the threshold voltage V_T and the width of the array determines its resistance R. Thus resistance and threshold voltage of 2D tunnel junction arrays can be optimized separately.

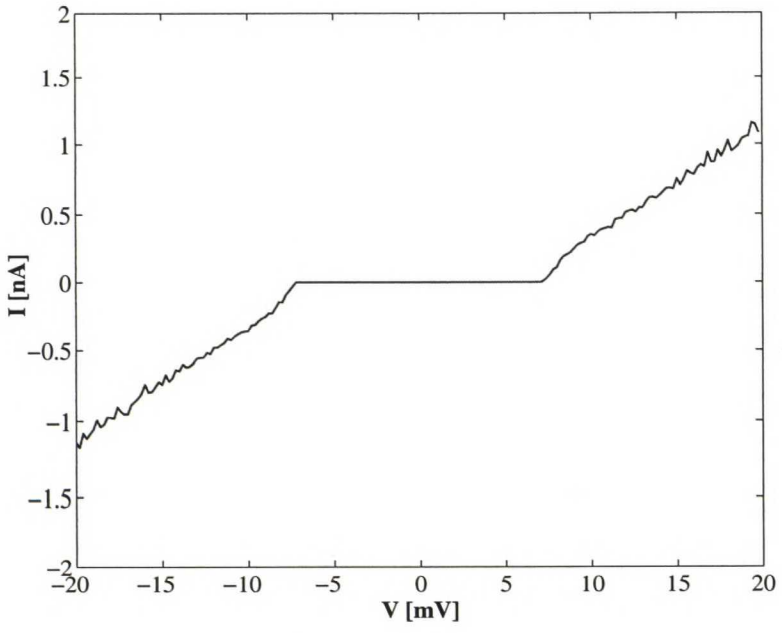

Figure 6.9: I-V curve of array of $N = 11$ tunnel junctions at $T = 0K$. All tunnel junctions are identical and also self capacitances are identical with each other. $R_T = 1.0 \cdot 10^6\Omega$, $C = 1.0 \cdot 10^{-16}F$ and $C_0 = 1.0 \cdot 10^{-18}F$.

6.8.3 Applications of Arrays.

One promising future application of tunnel junction arrays is the single electron memory circuit. An interesting possibility is to use single electron devices as a memory cells in circuits where the conventional CMOS technology is used in the peripheral circuit [44].

The conditions for a good single electron memory cell are [45, 46]:

- The memory cell must operate at room temperature or at least at the liquid nitrogen temperature (77 K).
- The bit-error rate must be reasonable.
- Robustness to random background charge.
- Low power consumption.

- Manufacturability.

6.9 Multigate Single Electron Transistor

A multigate SET can be considered as a realization of neuro SET. These floating gate structures can be adapted to common neural network architectures e.g. to cellular neural network (CNN) architecture. Furthermore multigate single electron transistor may provide means to overcame the degradation of switching speed of logic application of multi SET circuits [47, 48] and furthermore the use of multigate SETs reduce the number of transistors in some logic applications [49].

The equivalent circuit of a multigate single electron transistor is represented in figure 6.10. The drain-source current of the metallic two-gate SET is plotted in figure 6.12 at $T = 0\ K$ and in figure 6.13 at $T = 4.2\ K$. The other gate is used as a control gate with a constant voltage.

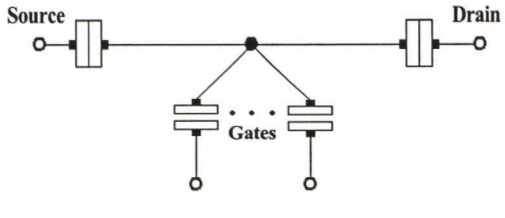

Figure 6.10: Equivalent circuit of multigate single electron transistor. Two gates are drawn.

6.10 Multigate SET XOR

There has been several experimental and theoretical studies of logic circuits based on single electron transistors [48, 50, 49, 47]. One possible exclusive OR (XOR) gate, which is based on multigate SET, is represented in figure

6.11. It has two input nodes i.e. the gates of the SET and the output node is the source of the SET. The switching characteristics of such a XOR gate is depicted in figure 6.14. It is seen that the drain-source current flows as a XOR function of the two gate voltages.

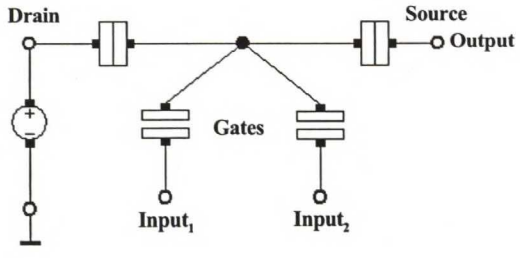

Figure 6.11: Equivalent circuit of a single electron transistor exclusive OR gate.

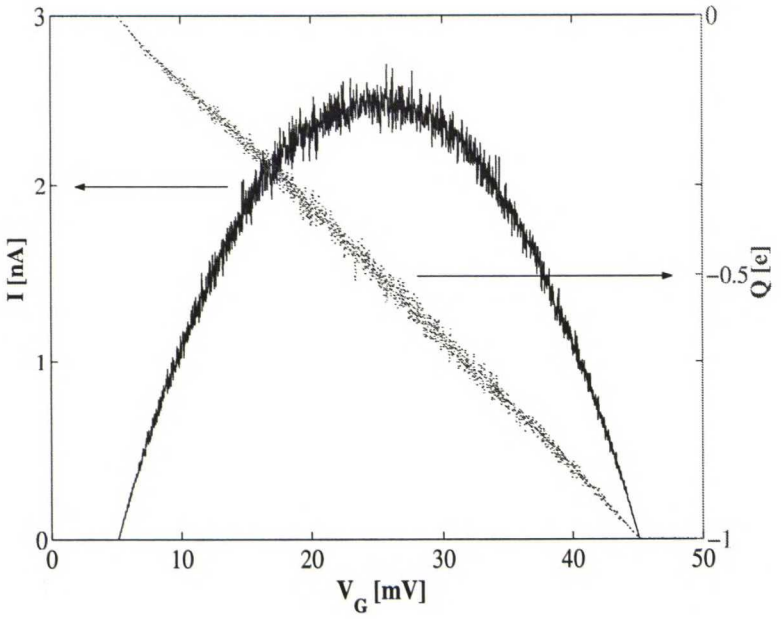

Figure 6.12: The drain-source current and the charge of the island of a two-gate SET as a function of the gate voltage at $T = 0\ K$. The voltage of the other gate is constant $V = 65\ mV$ and the drain-source voltage is $V = 10\ mV$. The tunneling and gate capacitances are $C = 1.0 \times 10^{-18}\ F$ and the tunneling resistances are $R = 1.0 \times 10^{6}\ \Omega$.

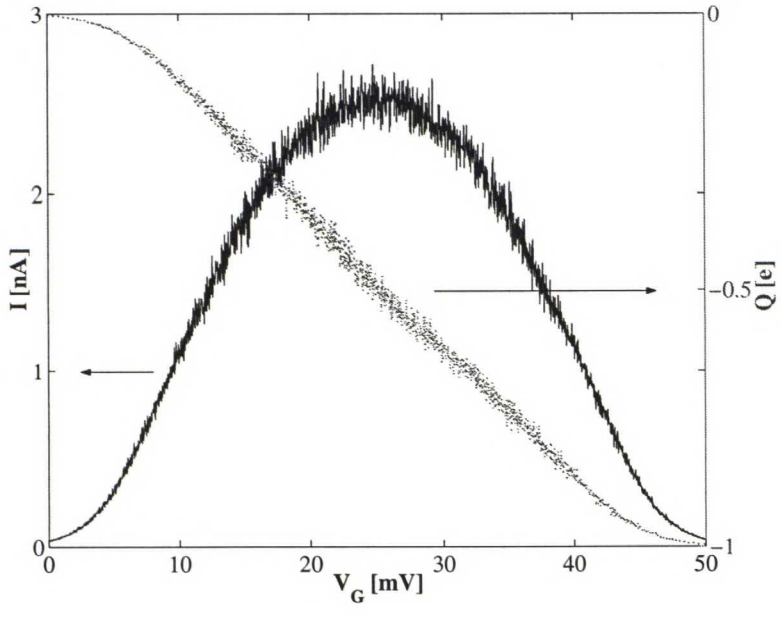

Figure 6.13: The drain-source current and the charge of the island of a two-gate SET as a function of the gate voltage at $T = 4.2\ K$. Parameters are the same as in figure 6.12.

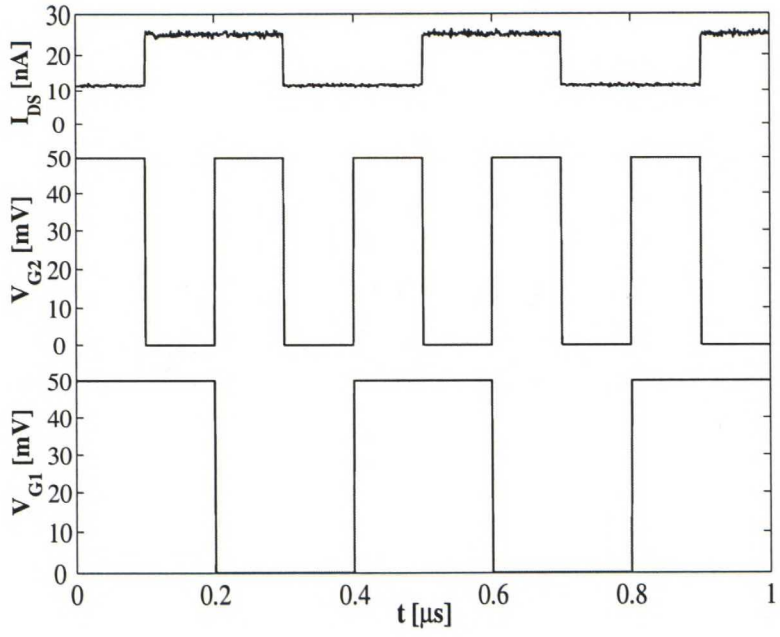

Figure 6.14: The switching characteristics of XOR gate at $T = 40\ K$. The drain-source voltage is $V_{DS} = 10\ mV$, the tunneling junctions have parameters $C = 10^{-18}$ F and $R_T = 10^5\ \Omega$ and the gate capacitances are $C_{G1} = C_{G2} = 2 \times 10^{-18}\ F$.

Chapter 7

Summary and Conclusions

In the first part of this master's thesis we have presented methods for calculation of transmission in channels where the quantum confinement is one- or two-dimensional. Also the relation between the transmission and conductance at zero and non-zero temperatures has been discussed within the Landauer-Büttiker formalism. We have furthermore calculated the conductances of the 2D and 3D channels in various geometries.

The latter part of this master's thesis deals with the Coulomb blockade and the Coulomb oscillations phenomena. We have also simulated selected single electron transistor based circuits by using the single electron device and circuit simulator called SIMON.

The step like behavior of conductance was seen in the analyzed rectangular constriction and in the silicon quantum point contact. The calculated conductances of the silicon QPC agree qualitatively with the measured results (see e.g. reference [51]).

The analysis of the constriction in a two-dimensional waveguide showed also clear resonance effects in each conductance step.

We have analyzed the operation of a SET as well as the operation of a multi-gate SET. Furthermore the multi-gate SET based exclusive-OR device was simulated as an example of logic application of devices that utilize the

Coulomb blockade and Coulomb oscillation phenomena. We also showed that with a proper choice of the capacitance and resistance values the Coulomb blockade behavior can also be detected at nonzero temperatures. The functionality of the XOR SET was simulated at $40K$.

We conclude that the SET circuits are a promising area of future logic circuits. The neuro-SET based neural networks might offer a fast and power efficient tool for signal processing. Furthermore remarkably high storage densities at low power consumption may be achieved with a SET based memory circuits.

Appendix A

Dirac's Bracket Notation

A.1 Definition

Let us consider two state functions $\psi(\mathbf{r})$ and $\phi(\mathbf{r})$. The representation independent notation called Dirac's bracket notation gives a monogram to the integral of the product of the two state functions as follows [52]:

$$\langle\psi|\phi\rangle = \int_{-\infty}^{\infty} \psi^*(\mathbf{r})\phi(\mathbf{r})\mathrm{d}\mathbf{r}. \tag{A.1}$$

The $\langle\psi|$ is called as a bra vector and the $|\psi\rangle$ is called as a ket vector. Their product $\langle\psi|\psi\rangle$ forms a bra-ket. If ψ and ϕ are such that

$$\int_{-\infty}^{\infty} \psi^*(\mathbf{r})\phi(\mathbf{r})\mathrm{d}\mathbf{r} < \infty \tag{A.2}$$

and c is any complex number, the following rules for integral operator (A.1) holds [52]:

$$\langle\psi|c\phi\rangle = c\langle\phi|\psi\rangle \tag{A.3}$$

$$\langle c\psi|\phi\rangle = c^*\langle\psi|\phi\rangle \tag{A.4}$$

$$\langle\psi|\phi\rangle^* = \langle\phi|\psi\rangle \tag{A.5}$$

$$\langle\psi + \phi| = \langle\psi| + \langle\phi| \tag{A.6}$$

$$\begin{aligned}&\int(\psi_1(\mathbf{r})+\psi_2(\mathbf{r}))^*(\phi_1(\mathbf{r})+\phi_2(\mathbf{r}))\mathrm{d}\mathbf{r}\\&=\langle\psi_1+\psi_2|\phi_1+\phi_2\rangle\\&=\langle\psi_1|\phi_1\rangle+\langle\psi_1|\phi_2\rangle+\langle\psi_2|\phi_1\rangle+\langle\psi_2|\phi_2\rangle.\end{aligned}\tag{A.7}$$

A.2 $\hat{\mathbf{r}}$ and $\hat{\mathbf{p}}$ Representations

The eigenstates of position operator $\hat{\mathbf{r}}$ are

$$\psi_{\mathbf{r}_0}(\mathbf{r})=\delta(\mathbf{r}_0-\mathbf{r}),\tag{A.8}$$

where $\mathbf{r}_0$ is continuous 3D variable. The states corresponding to $\mathbf{r}_0$ fulfill

$$\langle\mathbf{r}|\mathbf{r}'\rangle=\delta(\mathbf{r}-\mathbf{r}')\tag{A.9}$$

and

$$|\psi\rangle=\int\psi(\mathbf{r})|\mathbf{r}\rangle\mathrm{d}\mathbf{r},\tag{A.10}$$

where

$$\psi(\mathbf{r})=\langle\mathbf{r}|\psi\rangle.\tag{A.11}$$

Similarly the eigenfunctions of momentum operator $\hat{\mathbf{p}}$ are

$$\psi_{\mathbf{p}}(\mathbf{r})=\left(\frac{1}{2\pi\hbar}\right)^{3/2}e^{i\mathbf{p}\cdot\mathbf{r}/\hbar},\tag{A.12}$$

where $\mathbf{p}$ is continuous 3D variable and states corresponding to it obey

$$\langle\mathbf{p}|\mathbf{p}'\rangle=\delta(\mathbf{p}-\mathbf{p}')\tag{A.13}$$

and

$$\bar{\psi}(\mathbf{p})=\langle\mathbf{p}|\psi\rangle,\tag{A.14}$$

where

$$|\psi\rangle=\int\bar{\psi}(\mathbf{p})|\mathbf{p}\rangle\mathrm{d}\mathbf{p}\tag{A.15}$$

and $\bar{\psi}(\mathbf{p})$ is the Fourier transformation of wavefunction $\psi(\mathbf{p})$ corresponding to state $|\psi\rangle$.

Appendix B

Second Quantization

B.1 Occupation Number Formalism

The purpose of second quantization formalism [53, 54, 55] is to find simplified and systemized representation for the state vectors. In this occupation number representation one works with the state vectors which specify the single particle states which are occupied and uses creation and annihilation operators to change the occupancy of single particle states by one.

Let us begin by denoting the orthonormal basis of single particle states in lexical order as follows $|\alpha\rangle, |\beta\rangle, |\gamma\rangle, |\delta\rangle \ldots$. Next we construct the states of N-fermion system by using single particle states and occupation number formalism. The state of the N-particle system is specified by determining the N occupied single particle states: $\Psi = |\ldots, \mu, \nu, \ldots\rangle$.

B.2 Ladder Operators for Fermions

Ladder operators are introduced for characterizing the relationship between different occupation number states. The annihilation operator $\hat{a}_\mu$ annihilates or removes the single particle state $|\mu\rangle$ from occupied states. On the contrary,

the creation operator $\hat{a}_\mu^\dagger$ creates or adds the single particle state $|\mu\rangle$ into occupied states. Thereby the creation and annihilation operators are each others adjoint operators.

The formal definition of annihilation and creation operators for fermions are [53]:

$$\hat{a}_\mu^\dagger|\ldots,\lambda,\nu,\ldots\rangle = (-1)^{n_\mu}|\ldots,\lambda,\mu,\nu,\ldots\rangle \quad \text{(B.1)}$$

$$\hat{a}_\mu^\dagger|\ldots,\mu,\ldots\rangle = 0 \quad \text{(B.2)}$$

$$\hat{a}_\mu|\ldots,\lambda,\mu,\nu,\ldots\rangle = (-1)^{n_\mu}|\ldots,\lambda,\nu,\ldots\rangle \quad \text{(B.3)}$$

$$\hat{a}_\mu|\ldots,\lambda,\nu,\ldots\rangle = 0, \quad \text{(B.4)}$$

where n_μ is the number of occupied single particle states that lexically precede $|\mu\rangle$ in the adjacent $|\ldots,\lambda,\mu,\nu,\ldots\rangle$. The anticommutation rules for $\hat{a}_\mu$ and $\hat{a}_\mu^\dagger$ are:

$$\{\hat{a}_\mu\hat{a}_\nu\} = 0 \quad \text{(B.5)}$$

$$\{\hat{a}_\mu^\dagger\hat{a}_\nu^\dagger\} = 0 \quad \text{(B.6)}$$

$$\{\hat{a}_\mu\hat{a}_\nu^\dagger\} = \delta_{\mu\nu}. \quad \text{(B.7)}$$

These rules can be verified as follows:
Rule (B.5):

$$\{\hat{a}_\mu\hat{a}_\nu\}|\ldots,\mu,\nu,\ldots\rangle =$$
$$(-1)^{n_\mu}(-1)^{n_\nu-1}|\ldots\rangle + (-1)^{n_\nu}(-1)^{n_\mu}|\ldots\rangle = 0.$$

Rule (B.6):

$$\{\hat{a}_\mu^\dagger\hat{a}_\nu^\dagger\}|\ldots\rangle =$$
$$(-1)^{n_\nu}(-1)^{n_\mu}|\ldots,\mu,\nu,\ldots\rangle + (-1)^{n_\mu}(-1)^{n_\nu+1}|\ldots,\mu,\nu,\ldots\rangle = 0.$$

Rule (B.7) ($\mu \neq \nu$):

$$\{\hat{a}_\mu \hat{a}_\nu^\dagger\}|\ldots,\mu,\ldots\rangle =$$
$$(-1)^{n_\nu}(-1)^{n_\mu}|\ldots,\nu,\ldots\rangle + (-1)^{n_\mu}(-1)^{n_\nu - 1}|\ldots,\nu,\ldots\rangle = 0$$

$$\{\hat{a}_\mu \hat{a}_\mu^\dagger\}|\ldots\rangle =$$
$$(-1)^{n_\mu}(-1)^{n_\mu}|\ldots\rangle + 0 = 1 \cdot |\ldots\rangle$$

$$\{\hat{a}_\nu \hat{a}_\mu^\dagger\}|\ldots,\nu,\ldots\rangle =$$
$$(-1)^{n_\mu}(-1)^{n_\nu+1}|\ldots,\mu,\ldots\rangle + (-1)^{n_\nu}(-1)^{n_\mu}|\ldots,\mu,\ldots\rangle = 0$$

Other combinations of rule (B.7) are obvious.

B.3 Number Operator

An operator which operates in N-fermion system can be represented as a sum of single-particle operators that operate to certain single-particle state. Therefore an operator $\mathcal{O}$ can be written as

$$\mathcal{O} = \sum_\mu o_\mu, \tag{B.8}$$

where o_μ operates to single particle state $|\mu\rangle$. These operators can be written in basis $|\mu\rangle$ as

$$o_\mu|\mu\rangle = \sum_\alpha \langle\alpha|o_\mu|\mu\rangle|\alpha\rangle. \tag{B.9}$$

Now operating with $\mathcal{O}$ to multi-particle state leads us to sum of operations with single particle state operator o as follows:

$$\begin{aligned}&\mathcal{O}|\mu,\nu,\ldots,\omega\rangle = \\ &|o_\mu\mu,\nu,\ldots,\omega\rangle + |\mu,o_\nu\nu,\ldots,\omega\rangle + \ldots + |\mu,\nu,\ldots,o_\omega\omega\rangle.\end{aligned} \tag{B.10}$$

This can simplified further by substituting expansion (B.9) into above sum. Thus we obtain

$$\mathcal{O}|\mu,\nu,\ldots,\omega\rangle = \sum_\lambda \langle\lambda|o_\mu|\mu\rangle|\lambda,\nu,\ldots,\omega\rangle$$

$$
\begin{aligned}
&+ \sum_{\lambda} \langle \lambda | o_\nu | \nu \rangle | \mu, \lambda, \ldots, \omega \rangle \\
&\vdots \\
&+ \sum_{\lambda} \langle \lambda | o_\omega | \omega \rangle | \mu, \nu, \ldots, \lambda \rangle. \qquad \text{(B.11)}
\end{aligned}
$$

Realizing that by using correct annihilation and creation operators in each term of above sum we can modify it so that the original state ket appears in each term. Thus the simplified, ladder operators including, form of sum (B.11) is

$$
\begin{aligned}
\mathcal{O}|\mu, \nu, \ldots, \omega\rangle &= \sum_{\lambda} \langle \lambda | o_\mu | \mu \rangle \hat{a}_\lambda^\dagger \hat{a}_\mu | \mu, \nu, \ldots, \omega \rangle \\
&+ \sum_{\lambda} \langle \lambda | o_\nu | \nu \rangle \hat{a}_\lambda^\dagger \hat{a}_\nu | \mu, \nu, \ldots, \omega \rangle \\
&\vdots \\
&+ \sum_{\lambda} \langle \lambda | o_\omega | \omega \rangle \hat{a}_\lambda^\dagger \hat{a}_\omega | \mu, \nu, \ldots, \omega \rangle. \qquad \text{(B.12)}
\end{aligned}
$$

We can add terms into above sum corresponding to all possible states, because the corresponding annihilation operator has vanishing effect on unoccupied states as a result of its definition. Also λ goes trough every existing state due to expansion of operator o in equation (B.9). Thus operator $\mathcal{O}$ can be written as

$$
\mathcal{O} = \sum_{\lambda,\kappa} \langle \lambda | o_\kappa | \kappa \rangle \hat{a}_\lambda^\dagger \hat{a}_\kappa. \qquad \text{(B.13)}
$$

The number operator can now be obtained from $\mathcal{O}$ as a special case wherein $|\lambda\rangle$ are eigenfunctions of operators o i.e. $o_\lambda|\lambda\rangle = \varepsilon_\lambda|\lambda\rangle$. Therefore $\mathcal{O}$ simplifies into form

$$
\mathcal{O} = \sum_{\lambda} \langle \lambda | \varepsilon_\lambda | \lambda \rangle \hat{a}_\lambda^\dagger \hat{a}_\lambda = \sum_{\lambda} \varepsilon_\lambda \hat{a}_\lambda^\dagger \hat{a}_\lambda, \qquad \text{(B.14)}
$$

where the operator product $\hat{a}_\lambda^\dagger \hat{a}_\lambda |\lambda\rangle$ equals $|\lambda\rangle$ if the single-particle state is occupied and zero otherwise. This means that eigenvalues (i.e. number of fermions at $|\lambda\rangle$) of number operator for fermions are 0 and 1 as they, by Pauli exclusion principle, should be. If $\mathcal{O}$ is diagonal as in (B.13) it yields

$$
\mathcal{O}|\ldots\rangle = \sum_{\lambda} o_\lambda |\ldots\rangle = \sum_{\lambda} \varepsilon_\lambda |\ldots\rangle, \qquad \text{(B.15)}
$$

where λ goes trough every occupied single-particle state. This shows that $|\ldots\rangle$ is eigenstate of $\mathcal{O}$ with an eigenvalue which is a sum of the eigenvalues of o that corresponds occupied states. Thus we can define the total number operator as

$$\hat{N} = \sum_{\lambda} \hat{a}_{\lambda}^{\dagger} \hat{a}_{\lambda}. \tag{B.16}$$

Eigenvalues of this operator are the number of occupied single-particle states:

$$\hat{N}|\ldots\rangle = \sum_{\lambda} \hat{a}_{\lambda}^{\dagger} \hat{a}_{\lambda} |\ldots\rangle = N|\ldots\rangle. \tag{B.17}$$

B.4 Ladder Operators for Bosons

The bosonic ladder operators fulfill following commutation relations:

$$[\hat{a}_{\mu} \hat{a}_{\nu}] = 0 \tag{B.18}$$

$$[\hat{a}_{\mu}^{\dagger} \hat{a}_{\nu}^{\dagger}] = 0 \tag{B.19}$$

$$[\hat{a}_{\mu} \hat{a}_{\nu}^{\dagger}] = \delta_{\mu\nu}. \tag{B.20}$$

And as for fermions the number operator for bosons at state $|\mu\rangle$ is a product of creation and annihilation operators

$$\hat{N}_{\mu} = \hat{a}_{\mu}^{\dagger} \hat{a}_{\mu}, \tag{B.21}$$

whose eigenvalues n_{μ} give the number of bosons at state $|\mu\rangle$.

Bibliography

[1] T. Ando, Y. Arakawa, K. Furuya, S. Komiyama, and H. Nakashima. *Mesoscopic Physics and Electronics.* Springer-Verlag, 1998.

[2] J. Singh. *Physics of Semiconductors and Their Heterostructures.* McGraw-Hill, 1993.

[3] Juha Sinkkonen. Puolijohdeteknologian perusteet. Reports in Electron Physics 1996/11, 1996. Helsinki University of Technology.

[4] N. W. Ashcroft and N. D. Mermin. *Solid State Physics.* CBS Publishing Asia Ltd., 1976.

[5] Stephen Elliott. *The Physics and Chemistry of Solids.* Wiley, 2000.

[6] P. W. Atkins. *Physical Chemistry.* Oxford University Press, fourth edition, 1990.

[7] K. Barnham and D. Vvedensky, editors. *Low-Dimensional Semiconductor Structures, Fundamentals and Device Applications.* Cambridge University Press, 2001.

[8] S. Horiguchi, Y. Nakajima, Y. Takahashi, and M. Tabe. Energy eigenvalues and quantized conductance values of electrons in si quantum wires on (100) plane. *Jpn. J. Appl. Phys.*, 34(10):5489–5498, 1995.

[9] T. Dittrich, P. Hänggi, G.-L. Ingold, B. Kramer, G. Schön, and W. Zweger. *Quantum Transport and Dissipation.* Wiley-VCH, 1998.

[10] Y. Imry. *Introduction to Mesoscopic physics.* Oxford University Press, 1997.

[11] S. Datta. *Electronic Transport in Mesoscopic Systems.* Cambridge University Press, 1995.

[12] D. M. Young and R. T. Gregory. *A Survey of Numerical Mathematics.* Addison-Wesley Publishing Company, 1972.

[13] K. F. Riley, M. P. Hobson, and S. J. Bence. *Mathematical Methods for Physics and Engineering.* Cambridge University Press, 1997.

[14] J. Tulkki. Luentoja kvanttifysiikasta, 2003.

[15] A. Weisshaar, J. Lary, S. M. Goodnick, and V. K. Tripathi. Analysis and modeling of quantum wave-guide structures and devices. *J. Appl. Phys.*, 70(1):355–366, 1991.

[16] S. Horie and A. Suzuki. Mode coupling in ballistic wires with double constrictions. *J. Phys. Soc. Jpn.*, 71(1):204–210, 2002.

[17] D. K. Ferry and S. M. Goodnik. *Transport in Nanostructures.* Cambridge University Press, 1997.

[18] A. Weisshaar, J. Lary, S. M. Goodnick, and V. K. Tripathi. Analysis of discontinuities in quantum wavequide structures. *Appl. Phys. Lett.*, 55(20):2114–2116, 1989.

[19] R. B. Guenther and J. W. Lee. *Partial Differential Equations of Mathematical Physics and Integral Equations.* Dover, 1996.

[20] F. Sols, M. Macucci, U. Ravaioli, and K. Hess. Theory for a quantum modulated transistor. *J. Appll. Phys.*, 66(8):3892–3906, 1989.

[21] M. Macucci, A. Galick, and U. Ravaioli. Quasi-3-dimensional greens-function simulation of coupled electron wave-guides. *Phys. Rev. B*, 52(7):5210–5220, 1995.

[22] F. Sols. Scattering, dissipation, and transport in mesoscopic systems. *Annals of Physiscs*, 214(2):386–438, 1992.

[23] K. K. Likharev and K. A. Matsuoka. Electron-electron interaction in linear arrays of small tunnel junctions. *Appl. Phys. Lett.*, 67(20):3037–3039, 1995.

[24] C. P. Gerousis and S. M. Goodnick. Simulation of single-electron tunneling circuits. *Phys. Status Solidi B*, 233(1):113–126, 2002.

[25] K. K. Likharev. Single-electron devices and their applications. *P IEEE*, 87(4):606–632, 1999.

[26] H. Grabert and M. Devort, editors. *Single Charge Tunneling, Coulomb Blockade Phenomena in Nanostructures.* Plenum Press, 1992.

[27] Cristoph Wasshuber. *Computational Single-Electronics.* Springer-Verlag, 2001.

[28] P. Lafarge, H. Pothier, E. R. Williams, D. Esteve, C. Urbina, and M. H. Devoret. Direct observation of macroscopic charge quantization. *Z. Phys. B Con. Mat.*, 85(3):327–332, 1991.

[29] SIMON 2.0 (SIMulation Of Nano-structures) is single electron tunnel device and circuit simulator. Originally created at the institute for Microelectronics, TU Vienna, by Cristoph Wasshuber. See also [37] and [38].

[30] J. König, H. Schoeller, and G. Schön. Cotunneling and renormalization effects for the single-electron transistor. *Phys. Rev. B*, 58(12):7882–7892, 1998.

[31] Amnon Buxboim and Avraham Schiller. Current characteristics of the single-electron transistor at the degeneracy point. *Phys. Rev. B*, 67(16):165320, 2003.

[32] M. A. Kastner. The single-electron transistor. *Rev. Mod. Phys.*, 64(3):849–858, 1992.

[33] C. Gerousis, S. M. Goodnick, and W. Porod. Toward nanoelectronic cellular neural networks. *Int. J. Circ. Theor. App.*, 28(6):523–535, 2000.

[34] C. P. Robert and G. Casella. *Monte Carlo Statistical Methods.* Springer-Verlag, 1999.

[35] James E. Gentle. *Random Number Generation and Monte Carlo Methods.* Springer-Verlag, 1998.

[36] D. W. Heermann. *Computer Simulation Methods in Theoretical Physics.* Springer-Verlag, second edition, 1990.

[37] C. Wasshuber and H. Kosina. A single-electron device and circuit simulator. *Superlattice Microst.*, 21(1):37–42, 1997.

[38] C. Wasshuber, H. Kosina, and S. Selberherr. Simon - a simulator for single-electron tunnel devices and circuits. *IEEE T. Comput. Aid. D.*, 16(9):937–944, 1997.

[39] Michael Tinkham. *Introduction to Superconductivity.* McGrew-Hill, second edition, 1996.

[40] Walter A. Harrison. *Solid State Theory.* McGrew-Hill, 1970.

[41] R. L. Kautz, G. Zimmerli, and J.M. Martins. Self-heating in the coulomb-blockade electrometer. *J. Appl. Phys.*, 73(5):2386–2396, 1993.

[42] I. Lindell and A. Sihvola. *Sähkömagneettinen kenttäteoria 1. Staattiset kentät.* Otatieto, second edition, 1995.

[43] K. K. Likharev, N. S. Bakhalov, G. S. Kazacha, and S. I. Serdyukova. Single-electron tunnel junction array - an electrostatic analog of the josephson transmission-line. *IEEE T. Magn.*, 25(2):1436–1439, 1989.

[44] K. Yano, T. Ishii, T. Sano, T. Mine, F.Murai, T. Hashimoto, T. Kobayashi, T. Kure, and K. Seki. Single-electron memory for giga-to-tera bit storage. *PROC. IEEE*, 87(4):633–651, 1999.

[45] Ionnas Karafyllidis. Design and simulation of a single-electron random-access memory array. *IEEE T. Circuits-I*, 49(9):1370–1375, 2002.

[46] C. Wasshuber, H. Kosina, and S. Selberherr. A comparative study of single-electron memories. *IEEE T. Eelectron Dev.*, 45(11):2365–2371, 1998.

[47] M.-Y. Jeong, Y.-H. Jeong, S.-W. Hwang, and D. M. Kim. Performance of single-electron transistor logic composed of multi-gate single-electron transistors. *Jpn. J. Appl. Phys.*, 36(11):6706–6710, 1997.

[48] Y. Ono, H. Inokawa, and Y. Takahashi. Binary adders of multigate single-electron transistors: Specific design using pass-transistor logic. *IEEE T. Nanotechnol.*, 1(2):93–99, 2002.

[49] Y. Takahashi, A. Fujiwara, K. Yamazaki, H. Namatsu, K. Kurihara, and K. Murase. A multi-gate single-electron transistor and its applications to an exclusive-or gate. In *IEDM 98*, pages 127–130, 1998.

[50] Y. Takahashi, A. Fujiwara, K. Yamazaki, H. Namatsu, and K. Kurihara. Multigate single-electron transistors and their application to an exlusive-or gate. *Appl. Phys. Lett.*, 76(5):637–639, 200.

[51] M. Prunnila, S. Eränen, J. Ahopelto, A. Manninen, M. Kamp, M. Emmerling, A. Forchel, A. Kristensen, B. S. Sorensen, P. E. Lindelof, and A. Gustaffson. Silicon quantum point contact with aluminum gate. *Mat. Sci. Eng. B*, 74(1–3):193–196, 2000.

[52] Richard L. Liboff. *Introductory Quantum Mechanics*. Addison-Wesley, third edition, 1990.

[53] F. E. Harris, H. J. Monkhorst, and D. L. Freeman. *Algebraic and diagrammatic methods in many-fermion theory.* Oxford University Press, 1992.

[54] B. R. Judd. *Second quantization and atomic specctroscopy.* The Johns Hopkins Press, 1967.

[55] S. Doniach and E. H. Sondheimer. *Green's Functions for Solid State Physicists.* Imperial College Press, 1999.